Basin Research IAS EAGE

The synthetic seismic expression of Messinian salinity crisis from onshore records: implications for shallow- to deep-water correlations

Journal:	*Basin Research*
Manuscript ID	BRE-035-2018.R2
Manuscript Type:	Original Article
Date Submitted by the Author:	08-Mar-2019

Complete List of Authors:	Roveri, Marco; Parma University, Dipartimento di Scienze Chimiche, della Vita e della Sostenibilità Ambientale Gennari, Rocco; Università degli Studi di Torino, Dipartimento di Scienze della Terra Ligi, Marco; Research National Council of Italy, ISMAR-BO Lugli, Stefano; Università degli Studi di Modena e Reggio Emilia, Dipartimento di Scienze Chimiche e Geologiche Manzi, Vinicio; Universita' degli Studi di Parma, Dipartimento di Scienze Chimiche, della Vita e della Sostenibilità Ambientale Reghizzi, Matteo; Università di Parma, Dipartimento di Scienze Chimiche, della Vita e della Sostenibilità Ambientale

Keywords:	Messinian salinity crisis, synthetic seismic profiles, Balearic Promontory, evaporites, seismic stratigraphy

The synthetic seismic expression of Messinian salinity crisis from onshore records: implications for shallow- to deep-water correlations

Roveri M[a,*], Gennari R.[a], Ligi M.[b], Lugli S.[c], Manzi V.[a], Reghizzi, M.[a]

[a] Dipartimento di Scienze Chimiche, della Vita e della Sostenibilità Ambientale, University of Parma, Parco Area delle Scienze 157A, 43124 Parma (Italy)

[b] Istituto di Scienze Marine, CNR, Via Gobetti101, 40129, Bologna, Italy

[c] Dipartimento di Scienze Chimiche e Geologiche, University of Modena e Reggio Emilia, Via Campi 103, 41125 Modena (Italy)

*Corresponding author

E-mail address: marco.roveri@unipr.it

Keywords:

Messinian salinity crisis, synthetic seismic, Balearic Promontory, evaporites, seismic stratigraphy

ABSTRACT

The onshore-offshore correlation of sedimentary successions is a common problem in basin analysis, but it becomes critical for the full understanding of the Messinian salinity crisis (MSC), a complex array of palaeoenvironmental events which affected the Mediterranean basin at the end of the Miocene. The outcrop records show that the Messinian stratigraphic architectures may be highly complex as the deposits of the different MSC evolutionary stages can be lithologically similar and separated by erosional surfaces and/or morphostructural highs. The correct definition of the nature and stratigraphic position of Messinian deposits in offshore areas through seismic data may be almost impossible, especially where core data are sparse. To bridge

the gap between onshore and offshore records, we have built synthetic seismic sections from well-constrained outcrop successions. Our results provide useful insights and warnings for the interpretation of offshore data, pointing out that MSC units having different age, nature and depositional settings, may show similar seismic facies and geometries. Conversely, the same deposit may result in different seismic facies, either with parallel and high-amplitude ~~reflectors~~ reflections or even transparent or chaotic due to interference patterns of seismic reflections related to dominant frequency. It follows that a correct interpretation of the nature and age of deep-seated Messinian deposits can only be obtained through the integration of seismic and core data, and ~~taking into account~~considering the onshore record. The application of our approach to the Balearic Promontory results in an alternative ~~scenario~~ interpretation with respect to previous models. We show that this offshore area has ~~perfect~~ good analogues in the onshore of the Betic Cordillera and includes both shallow and intermediate depth sub-basins that underwent a strong post-Messinian subsidence.

1. INTRODUCTION

At the end of the Miocene the Mediterranean basin and its surrounding areas underwent severe environmental modifications due to the narrowing and/or closure of Mediterranean-Atlantic gateways in the Gibraltar strait area (Krijgsman et al., 2018). The Mediterranean hydrological balance changed accordingly and the result was the periodic accumulation of huge volumes of evaporites (sulfates, halite and K-Mg salts) in both shallow and deep sub-basins. Meanwhile, the Mediterranean shelves and slopes underwent widespread erosion. This is commonly related to fluvial rejuvenation caused by an evaporative base-level drop of 1500 m (Hsü et al., 1973). This event, known as the Messinian salinity crisis (MSC; see Table 1 for a list and explanation of the acronyms used in this paper), started at 5.97 Ma (Manzi et al., 2013) and ended abruptly at 5.33 Ma (*i.e.*, at the base of the Pliocene) with the full re-establishment of the Atlantic connections. The MSC had important consequences for the marine and continental biota of the peri-Mediterranean area. For all these reasons, the full comprehension of MSC events has always drawn the attention of a large scientific community. However, after almost 50 years of extensive studies, the changes underwent by marine and terrestrial environments, as well as ~~what really happened and~~ their causes, ~~of these events~~ are still not fully understood. This is due to the difficulty of correlating onshore and offshore successions, a necessary stop for reconstructing a comprehensive stratigraphic framework. Nevertheless, considerable advancements have been recently achieved by onshore studies, which has resulted in the proposition of a three stages MSC evolutionary scenario (CIESM, 2008; Roveri et al., 2014a; see Chapter 2).

On the other hand, the offshore record is mainly known through geophysical data; DSDP and ODP cores have recovered on average only a few tens of meters ~~the very~~at the top of the deep offshore salt giant (see Roveri et al., 2014b and Lugli et al., 2015). Recently, well logs and cuttings made available by oil companies allowed ~~to~~ dating of~~e~~ the onset of MSC and of evaporite deposition (Manzi et al., 2018; Melijson et al., 2018), and the top of the main evaporitic body in the Eastern Mediterranean (Gvirtzman et al., 2017). Despite these important results, on-average low seismic resolution and scarce core~~s~~ data still hamper the full understanding of Messinian events, thus fueling lively controversies and several contrasting scenarios (Roveri et al., 2014a).

A great effort is needed to improve correlations along a depositional profile (*i.e.* referred to the paleodepths at the MSC onset) from marginal, including shallow (< 200 m) and intermediate (200-1000 m), to deep settings (> 1000 m) (~~Fig. 1~~see Roveri et al., 2014a, their figure 4). Shallow- and intermediate-water deposits (Roveri et al., 2001; 2008c; Manzi et al., 2005; 2007; see Roveri et al., 2014a, their figure 14~~Fig. 2~~), which are usually incomplete due to the strong Messinian erosion (Ryan and Cita, 1978; Lofi et al., 2005), can be found in both present-day onshore and offshore settings. Conversely, Messinian deep-water successions, which are more continuous and expanded, are preserved only offshore, below the Mediterranean abyssal plains~~ (Fig. 2)~~. Stratigraphic accuracy and resolution are ~~greatly~~ very different when looking at outcropping or buried successions. Integration of field, seismic and borehole data has been successfully carried out onshore (Sicily, Apennines, Spain, Cyprus), resulting in high-resolution chronostratigraphic reconstructions (Roveri et al., 2001; 2003; 2005, 2006a,b; 2008a; 2009; Omodeo-Salé et al., 2012; Manzi et al., 2007; 2011; 2016a; Dela Pierre et al., 2011; Soria et al., 2008; Corbi et al., 2016). These studies documented the rapid lateral and vertical facies changes and the subaerial and subaqueous erosional surfaces of the Messinian successions. The high seismic velocities of evaporites and the frequently observed physical disconnection of the Messinian deposits make subsurface reconstructions very difficult, especially in the case of low seismic resolution and lack of core data.

How can these problems be solved?

The novel approach adopted in this paper ~~consists in~~involves the reconstruction of synthetic seismic sections that ~~provide~~ allows the seismic expressions of outcropping units to be compared with the offshore records (Fig. ~~2~~1).

We apply this technique to the Betic Cordillera ~~(BC)~~ and Sicily basins focusing on the deposits that may produce seismic units of ambiguous interpretation. We then compare our results with a detailed analysis of the MSC record of the Balearic Promontory (~~BP,~~ southeastern Spain). This offshore area offers the opportunity to correlate shallow, intermediate and deep Messinian settings, thus representing a key area for the reconstruction of MSC events.

2. MSC STRATIGRAPHY: AN OVERVIEW

Onshore, the MSC developed during three distinct evolutionary stages showing peculiar palaeoenvironmental conditions and evaporitic deposits (Fig. ~~4~~2). Integrated stratigraphy and $^{87}Sr/^{86}Sr$ data constrain these deposits into a high-resolution chronostratigraphic framework which is summarized here (Hilgen et al., 2007; CIESM, 2008; Roveri et al., 2014a).

2.1. MSC onset and stage 1 (5.97-5.60 Ma)

The MSC onset occurred at 5.971 Ma within the 4th precessional cycle above the C3An.1n-C3r magnetic reversal (Manzi et al., 2013) and was synchronous throughout the entire Mediterranean basin (Krijgsman et al., 1999; Manzi et al., 2013; 2018; Roveri et al., 2014a). It corresponds to either the base of the lowermost primary *in situ* evaporites (gypsum or anhydrite) or the conformable surface (here defined Onset Surface - OS; Figs ~~4~~2, ~~5a~~3a-d) marking the rapid disappearance of normal marine foraminifera assemblages (Manzi et al., 2007, 2018; CIESM, 2008, Gennari et al., 2013; 2018; Roveri et al., 2014a). The MSC onset not always coincides with the base of primary *in situ* evaporites (Primary Lower Gypsum-PLG; Figs 2,~~.~~ ~~5a~~3a-b), which may be locally much younger or even missing (Manzi et al., 2007; 2016; 2018; Roveri et al., 2016; Dela Pierre et al., 2011; Fig. ~~5a~~3a,c,d). Thus, the base of the PLG (here defined Evaporite Onset Surface - EOS) is diachronous and not necessarily coincident with OS. According to Lugli et al. (2010), the PLG unit, with thickness ranging between 140 and 250 m, formed only in shallow and silled marginal basins and includes up to 16 gypsum-mudstone precession-controlled cycles (Fig. ~~5a~~3a; Vai, 1997; Krijgsman et al., 1999). The 5 lowermost cycles consist of massive and banded selenite beds (Vai and Ricci Lucchi, 1977) with sharp bottom and top surfaces (Fig. ~~5a~~3a); cycles 1 and 2 are the thinnest (a few meters), conversely, cycles 3-5 are the thickest (up to 40 m; Fig. ~~5a~~3a). The uppermost cycles (6-16) show i) intermediate thickness, ii) peculiar gypsum facies (branching selenite, supercones; Dronkert, 1976; Lugli et al., 2010), iii) irregular top surfaces and iv) abrupt internal lateral transitions to fine-grained sediments (marls) which locally may provide discontinuous internal geometry (Fig. ~~5e~~3e,f).

Toward their landward and basinward terminations, the gypsum beds become thinner and discontinuous, changing into lenticular geometries (Fig. ~~5g~~3g) and pinching-out abruptly. In shallower settings PLG evaporites are laterally replaced by limestones (Manzi et al., 2013; Fig. ~~5c~~3c) and/or coastal hybrid carbonate-siliciclastic deposits (Terminal Carbonate Complex – TCC; Cornée et al., 2004; Conesa et al., 1999; Roveri et al., 2009; Bourillot et al., 2010). In deeper settings they are replaced by foraminifera-barren, organic-rich shales interbedded with thin dolomitic limestone (FBI – foraminifer-barren interval; Manzi et al., 2018) attaining a maximum thickness of 50-60 m (Manzi et al., 2007; 2018; Dela Pierre et al., 2011). As a consequence, the OS surface may correspond to the base of either the PLG (thus coinciding with the EOS) or their shallow- and/or deep-water evaporite-free equivalents (Fig. ~~5a~~3a,d).

An erosional surface, showing ~~with~~ evidence of subaerial exposure in more marginal areas, commonly truncates the PLG unit. This unconformity is the most important and evident Messinian key surface and is known in the literature as the MES, ~~(~~Messinian (or Marginal; Lofi et al., 2011) Erosional Surface ~~– MES;~~ (Table 1; Figs 2,~~.~~ ~~5h~~3h,i) ~~commonly truncates the PLG unit~~.

2.2 MSC Stage 2 (5.60-5.54 Ma)

The MSC stage 2 is characterized by a more heterogeneous stratigraphic architecture than stage 1. Evaporite-bearing deposits (Resedimented Lower Gypsum unit – RLG; Fig. ~~4~~2) including halite, gypsum primary cumulates and/or clastic gypsum deriving from the dismantlement of the PLG unit, accumulated in physically disconnected and deeper depocenters (Clauzon et al., 1996; Manzi et al., 2005; CIESM, 2008).

As previously stated, t~~T~~he beginning of stage 2 is marked by the MES, an erosional surface developed ~~widespread at a regional-scal~~throughout ~~e~~ the Mediterranean margins ~~erosional subaerial settings (MES-su;~~ in both subaerial (Fig. 3h-i) and ~~. This surface passes downslope into a~~ suba~~e~~queous ~~unconformity~~conditions (~~;~~ Fig. 4a,d,e,f), and by its ~~, more distally,The subaerial unconformity (MES)~~MES, which ~~truncates and exposes to subaerial erosion the PLG unit, truncating the PLG unit passes downslope into a subaqueous unconformity flooring the RLG (Fig. 6a~~4a~~) and, more distally, to its~~a correlative conformity (MES-CC; Fig. ~~6b~~4b) in the deep basins. The RLG unit shows erosional internal surfaces, associated with coarse-grained gravity flow deposits and/or halite (Fig. ~~6a~~4a,b,e,f), which merge upslope into the MES. The RLG top can be conformable in the depocenters and/or erosional or irregular on the basin flanks (Fig. ~~7a~~5a,b). The unit may include chaotic deposits representing subaqueous mass failures and olistostromes accumulated at the base of the slopes or within canyons (Lugli et al., 2013). They consist of disarticulated and folded shales, gypsarenites and PLG olistoliths (Fig. ~~6d~~4d; Manzi et al., 2005; Roveri et al., 2006a,b; 2008b,c). The PLG deposits, due to the high mechanical contrast with underlying shales, were in fact prone to large-scale failures. PLG olistoliths can be few hundred meters wide and up to 100 m thick and commonly rest horizontally on the basin floor, conditions which simulate in-place successions and may prevent their recognition as eradicated blocks. These chaotic deposits have irregular basal and top surfaces (Fig. ~~6f~~4f; ~~7a~~5a) and can be onlapped by stratified clastic gypsum (*e.g*. gypsum turbidites; Fig. ~~6e~~4e; ~~7~~5) or even by stage 3 deposits (Fig. ~~7a~~5a; Roveri et al., 2003; 2006b; Manzi et al., 2011).

In Sicily, as well as in Calabria (Crotone Basin; Roveri et al., 2008c), the RLG unit includes thin (tens of meters) to thick (up to 400 m) lenticular halite bodies (Fig. ~~6a~~4a) accumulated in intermediate water depth sub-basins. The RLG deposits are usually detached from the PLG through intervening structural highs that may be very narrow (a few km across; see examples in Roveri et al., 2003; 2006a,b; Figs. ~~4~~ 4 and ~~13~~10). In these cases, the stratigraphic relationships between the two evaporite-bearing units are defined by tracing the MES from the top of the PLG deposits to the base of the RLG unit.

2.3 MSC Stage 3 (5.54-5.33 Ma)

In basinal settings, the RLG unit is conformably overlain by the uppermost Messinian deposits, which record a generalized hydrological change toward more diluted waters (“Lago-Mare” phase; Orszag-Sperber, 2006; Rouchy and Caruso, 2006; Roveri et al., 2014a; Stoica et al., 2016; Fig. 2). At the basin margins, these deposits can seal the MES unconformity, onlapping the eroded PLG (Fig. 2; Roveri et al., 2008a; Manzi et al., 2009).

Stage 3 deposits are thicker and more complete in the intermediate-depth depocenters than those of the previous stages; they usually show a tabular geometry and a precession-driven cyclic stacking-pattern (Vai, 1997; Roveri et al., 2008a; Krijgsman et al., 1999). The cycles consist of alternation of primary evaporites (Upper Gypsum - UG) and mudstones in marginal basins of Sicily and Eastern Mediterranean (Cyprus, Crete), with a maximum thickness of 200 m (Eraclea Minoa; Manzi et al., 2009). The UG evaporites are differing from the PLG in terms of i) facies (absence of branching selenite), ii) bed thickness (<10 m), iii) number of cycles (7) and iv) $^{87}Sr/^{86}Sr$ signature (<0.709088; Roveri et al., 2014b). The top of the gypsum beds can be irregular, due to the local development of domal structures (Fig. ~~8a~~6a,b). In the western Mediterranean and Northern Apennines, stage 3 cycles are evaporite-free and formed by alternation of fine and coarse-grained fluvio-deltaic systems in the shallow depocenters (Fig. ~~8c~~6c) and turbidite systems in deeper settings. The thickness of these deposits is highly variable ranging from less than 50 m in deep areas, away from the clastic input, to up to 1000 m (Po basin, Northern Apennine foredeep, Laga Basin; Roveri et al., 2006a,b). The upper boundary witness the return to normal marine conditions at the base of the Pliocene and consists of a flat surface associated with a sharp lithological boundary (Fig. ~~8d~~6d,e), or a quite subtle transition within a mudstone succession (Fig. ~~8f~~6f) and marked by an organic-rich horizon (Gennari et al., 2008; Fig. ~~8g~~6g).

2.4 The MSC offshore record

The seismic markers defined offshore (Lofi et al., 2011a,b; Maillard et al., 2014; Fig. 1~~; Fig. 2~~) lack reliable time and sedimentological constraints and can be only tentatively compared with the onshore ones (Fig. ~~3~~1). The classic deep basin MSC trilogy, given by the alternation of high-amplitude, laterally continuous and parallel reflectors (the "*bedded*" unit of Lofi et al., 2011a,b; Maillard et al., 2014) and transparent units (*i.e.* LU – Lower Unit - bedded, MU – Mobile Unit - transparent, UU – Upper Unit - bedded; see Fig. ~~2~~1), has long been correlated (Hsü et al., 1973) with the onshore Sicilian threefold succession: Lower Gypsum/Halite/Upper Gypsum. Conversely, recent works (Roveri et al., 2008b; 2014c) suggested that 1) the Lower Gypsum has no evaporitic equivalent in deep basins and 2) the Upper Gypsum would correspond only to the topmost part of the UU unit. Moreover, in areas where the MU unit is absent or too thin to be detected, the record consists of a "*bedded*" unit (BU), whose nature and stratigraphic position is uncertain. As a consequence, the largest volume of evaporites in deep offshore areas would belong to stage 2, as recently argued for the Eastern Mediterranean (Manzi et al., 2018).

The stage 3 deposits are the only ones relatively well-known also in offshore settings, where DSDP-ODP cores recovered the top of the MSC units. These deposits mainly consist of shales and usually show a thickness not exceeding a few tens of meters; it follows that they can be hardly distinguished in low-resolution seismic profiles (*e.g.*, Gvirtzman et al., 2017; Roveri et al., 2014b) where they are included, together with stage 2 deposits, within the UU unit. Locally, as in the Tyrrhenian basin, the stage 3 deposits are thicker and may include m-thick cumulate or clastic gypsum beds (Roveri et al., 2014c; Lugli et al., 2015). In this case a correspondence between UU and onshore shallow UG deposits can be established (~~Fig. 9~~see Roveri et al., 2014b, their figure 8).

3. TRANSLATING THE ONSHORE RECORD INTO SEISMIC UNITS: A SEISMIC FORWARD MODELLING EXPERIMENT

In this section we describe the geophysical characteristics of units and surfaces of the three MSC stages. To this purpose, we selected onshore basins (Sorbas and Nijar in the Betic Cordillera, Southern Spain, and Belice in Sicily) with chronostratigraphic constraints and stratigraphic architectures more relevant for a comparison with the offshore record. First, we provide an overview of these three basins including new field data. Then, on the basis of published geological cross-sections, we reconstruct a set of synthetic seismic sections.

3.1 Dataset

3.1.1 Sorbas-Vera basin ~~***(SVB)***~~. The Sorbas basin formed during the Miocene in the external zone of the Betic Cordillera (~~BC;~~ Fig. ~~10a~~7a; Krijgsman et al., 2001; Braga et al., 2006; Roveri et al., 2009). It was bounded to the north and to the south by basement ridges (Sierra de Los Filabres and Sierra Cabrera, respectively) on top of which carbonate platforms developed before and during the crisis (Martin and Braga, 1994; Riding et al., 1998; Conesa et al., 1999; Braga et al., 2006; Roveri et al., 2009; Bourillot et al., 2010). The Sorbas basin was connected to the open Mediterranean Sea through the Sierra Cabrera sill (Fig. ~~10a~~7a). To the east, a sill and a narrow corridor connected it to the deeper Vera basin (Braga et al., 2001), thus forming a single, larger basin (Sorbas-Vera Basin) that can be subdivided into four sectors with different Messinian stratigraphy (Fig. ~~10b~~7b,d~~c~~).

The PLG evaporites of stage 1 accumulated only in the shallow~~est~~ sector 1 of the Sorbas-Vera Basin ~~B-1 sector~~, bounded to the north and to the south by pre-crisis reefs (Braga et al., 2006) passing downslope into hemipelagic marls (Abad marls; Sierro et al., 2001). As a consequence, the PLG evaporites formed in a silled basin *beyond* the reef edge at an estimated maximum depth of ~240 m by Riding et al. (1998).

Fast deposition of gypsum led to the partial infill of the basin, which had a palaeodepth of 60-70 m at the end of stage 1, based on the thickness of the overlying prograding coastal to deltaic deposits. These deposits belong to the Sorbas Member~~b~~ (Roep et al., 1998; Fig. ~~10c~~7d~~c~~) that records MSC stage 2 and the lower stage 3 (Roveri et al., 2009).

The upper stage 3 is recorded by the continental deposits of the overlying Zorreras member. Only minor, low-relief erosional surfaces are locally observed, especially in the Zorreras Mb. Mixed siliciclastic-carbonate platforms with abundant microbialites (Terminal Carbonate Complex) represent the lateral equivalents of the Sorbas Mb. along basin margins. The transition to the Pliocene is marked by an abrupt facies change from the reddish silts of the Zorreras Mb. (Fig. ~~8e~~6e,f) to nearshore deposits (grey marls and calcarenites with marine shell layers; Roveri et al., 2018).

In~~ the SVB-2 ~~sector 2 (Fig. ~~10b~~7b,d~~c~~) the MSC deposits are absent and the upper Tortonian-lower Messinian Azagador and Abad members (*i.e.*, pre-MSC) consist of deeper water deposits with respect to sector 1 (Braga et al., 2001).

~~The SVB-3 s~~Sector 3 (Fig. ~~10b~~7b-d~~,c~~) is characterized by gypsum-bearing chaotic bodies (the Garrucha and Coscojar olistrostromes; Fortuin et al., 1995; Barragan, 1986; Braga et al., 2006; Di Blasi, 2018; Fig. ~~11~~3g-i~~8~~), emplaced above a deeply scoured surface cutting lower Messinian and older units as well as the local basement (Fig. ~~11a8a~~7c). These chaotic deposits form high-relief topographic features with an irregular top surface draped by Pliocene hemipelagic marls (Fortuin et al., 1995). Our observations reveal that the gypsum deposits consist of selenite olistoliths and gypsarenite-gypsrudite beds (Fig. ~~11b8b,d-g~~3g-i). New $^{87}Sr/^{86}Sr$ analyses (Fig. ~~11c~~S14) confirm that these evaporites derived from a PLG source (Lugli et al., 2010; Reghizzi et al., 2017) and were emplaced subaqueously as olistostromes and/or debrites (Fortuin et al., 1995).

In ~~SVB-~~sector 4 (Fig. ~~10b~~7b) pre-MSC turbidites (*e.g.*, the "Santiago Beds") are directly overlain through the MES by a thin (< 20 m; Fortuin et al., 1995) turbiditic unit belonging to stage 3 (Volk, 1967; Barragan, 1986; Montenat, 1990; Stoica et al., 2016), in turn capped by lower Pliocene marls with thin, lenticular sandstone bodies (Fig. ~~8h~~6h).

In our reconstruction of the Sorbas-Vera Basin, the ~~SVB-~~sector 2 is a steep slope area, likely representing the upper reach of a pre-MSC canyon or submarine valley, rejuvenated and connected to an ancestor of the present-day Almanzora-Alias-Garrucha canyon (Gomez de la Peña et al, 2016); the ~~SVB~~sector ~~-~~3 includes the canyon mouth and the transition to a depositional zone developed in an intraslope basin (*e.g.* ~~SVB~~sector ~~-~~4; compare with the Cabo de Gata and Almanzora-Alias-Garrucha canyons; Gomez de la Peña et al, 2016).

3.1.2 Nijar basin ~~***(NB)***~~. The Nijar Basin is separated from the Sorbas-Vera Basin by the Sierra Cabrera and Sierra Alhamilla ridges and is bounded to the south by Sierra del Cabo de Gata. In this basin, as in the Sorbas-Vera Basin, the MSC stage 1 is represented by the PLG (Yesares Member~~b~~) but, differently, the PLG is cut by deep incisions filled by a chaotic body made up of disarticulated PLG blocks and stratified gypsarenites (Fortuin & Krijgsman, 2003; Omodeo-Salé et al., 2012), representing the local expression of stage 2 RLG deposits. The vertical and lateral transition between the PLG and the RLG units across the MES erosional surface occurs over a very short distance (hundreds of meters to a few kilometers; see Fig. ~~13~~10). Stage 3 is represented by the coastal, deltaic to continental deposits with the typical Lago-Mare fossil assemblage of the Feos Formation (Bassetti et al., 2006). This unit shows a well-developed cyclical stacking-pattern given by the alternation of m-thick tabular conglomeratic and white marls bodies showing a good lateral continuity (Omodeo-Salé et al., 2012). Similarly to the Sorbas-Vera Basin, the transition to the Pliocene is marked by an abrupt facies change from the fluvio-deltaic Feos Formation~~m.~~ (Fig. ~~8c~~6c,d) to the marine deposits (nearshore calcarenites).

3.1.3 Belice Basin ~~***(BB)***~~***.*** This basin of western Sicily offers one of the best examples of the complex architecture of the RLG deposits and of their relationships with stage 1 PLG evaporites (Roveri et al., 2006b). Here the RLG unit consists of tabular, horizontally stratified turbiditic gypsarenite bodies embedding chaotic masses of mudstones and folded gypsarenites beds with giant PLG olistoliths (Fig. ~~7c~~5c-f; Roveri et al., 2006a,b). The RLG deposits onlap against the eroded southern flank of a thrust-related antlicline forming the northern margin of the basin and are overlain by Pliocene marine deposits through an irregular surface with no evidence of subaerial exposure (Trubi Formation~~m.~~; Fig- ~~7b~~5b). The anticline preserves in its northern flank *in situ* PLG deposits cut by an erosional surface sealed by Pliocene marine deposits.

3.2 Seismic forward modelling – Abridged Methods

The selected geological cross-sections (Fig.~~s S1, S2, S3~~8) show an alternation of high and low seismic velocity layers (marls, evaporites and shales, limestones, sandstones and conglomerates), erosional surfaces, steep clinoforms, faulted and/or folded blocks. For the different lithologies we have used average density and P-wave velocity values from the literature (~~reported in Figs S1, S2, S3~~Table 2). A number of forward modelling methods are available; we simulated stacked seismic sections adopting the image ray-approximation (Fagin, 1991), that uses zero-offset travel-time modelling based on normal incidence tay-tracing. After having built geological models including ~~depth~~ smoothed horizons in depth, P-wave velocities and densities, we have constructed synthetic seismograms to identify seismic reflections within a true zero-offset section with constant trace-spacing. Finally, the zero-offset section is time ~~-depth~~ migrated in order to ~~locate correctly~~ move reflectors in their true subsurface positions and to collapse diffractions ~~at depth~~ (see full methodology in Supplementary Information). A variable color density display has been created by assigning different densities of shading to different amplitude values (positive, black; negative, red). Higher amplitudes are shaded darker, while lower amplitudes are less dark. We have created synthetic sections with different Common ~~Depth~~Mid Points~~CDPs~~ (C~~D~~MPs')~~'~~ spacing (3.125, 6.25, 12.5 and 25 m) and dominant frequencies (f_M = 40, 60, 120, 180, 250 and 500 Hz) in order to test horizontal and vertical resolution. The synthetic seismic sections of figures ~~12~~9, ~~13~~ 10 and ~~14~~ 11 have C~~D~~MPs' spacing of 3.125 m and are shown with 60 and 180 Hz dominant frequencies. For some key ~~tracts~~ portions of the sections, all the frequencies tested are shown.

3.3 Seismic forward modelling – Results

3.3.1. MSC onset and stage 1. The PLG deposits shown in the synthetic seismic sections (Figs 8a-c, ~~12~~9, ~~13~~10, ~~14~~11; Table ~~1~~2) form seismic units with P-wave interval velocity ranging between 4.0 and 4.5 km/sec, according to the relative thickness of gypsum-anhydrite and shale beds. Their base is defined by the high acoustic impedance contrast with the underlying deposits. The much higher accumulation rate of gypsum with respect to its lateral shallow-water equivalents may result~~s~~ in an apparent onlap, that simulates an unconformable base, as shown in the SVB (Fig. ~~12b~~9b,c,f-i).

The Sorbas-Vera Basin sections (Fig. 8a, ~~12~~9) show~~s~~ that the PLG unit is entirely characterized by a seismic facies with high-amplitude parallel reflectors (*"bedded"*) only at dominant frequencies ≥ 180 Hz, that allow a vertical resolution~~s~~ ≤ 6 meters. At lower frequencies (below 120 Hz; vertical resolution ~8m), the entire unit (Fig. ~~12b~~9b,d-e) or its upper part (Fig. ~~12f~~9f), including gypsum cycles less than 6 m thick on average, may appear as irregularly-bedded (simulating internal erosional surfaces) or even chaotic. This is due to interference patterns related to the thickness of individual cycles and is particularly evident for the uppermost (e.g. 10 to 15) thinner and more discontinuous cycles (Fig. ~~5e~~3e-g) and at frequencies as low as 40 or 60 Hz (vertical resolution ~ 25 m and 16 m, respectively). The full resolution of each individual cycle~~s~~ is obtained at 500 Hz, allowing a vertical resolution of ~2 m (Fig. ~~12i~~9i).

Furthermore, the peculiar stacking pattern of the gypsum cycles, with thinner layers at the lower and upper parts, may simulate internal discordances (Fig. ~~12f~~9f-i). Thickest (up to 40 meters) cycles (3-5) may appear as seismically transparent intervals and thus misinterpreted for halite-bearing or chaotic units (Fig. ~~12f~~9f-i).

Commonly, the PLG top surface is erosional (MES) and/or locally associated with angular discordances (Nijar ~~B~~ and Belice basins~~B~~, Figs 8b,c, ~~13~~10, ~~14~~11; Northern Apennines, Roveri et al., 2003; 2006a); it follows that the PLG thickness can be significantly reduced in respect to the complete successions. In the Sorbas-Vera Basin basin depocenter the upward transition to stage 2 is continuous and the marly and sandy Sorbas member conformably overlays the PLG evaporites; as a consequence, the top surface appears as a high amplitude, continuous reflector. A typical blocky pattern makes the PLG easily recognizable in well logs (Lugli et al., 2010; Fig. ~~5a~~3a); the presence of two thinner overlain by three-four thicker cycles indicates that the PLG unit is complete at its base.

3.3.2 MSC stage 2. The seismic expression of stage 2 units is shown in the Nijar~~B~~ Basin and Belice Basin~~B~~ sections (Figs 8b,c, ~~13~~10,~~14~~11); the stratified RLG deposits made of gypsum turbidites and/or carbonate breccia, form a "*bedded*" seismic facies (parallel, high-amplitude reflectors), hardly distinguishable from the PLG one. P-wave interval velocity of the RLG units can be highly variable, ranging between 2.7 and 4.5 km/sec., according to their prevailing lithology. The PLG and RLG deposits commonly occur in distinct depocenters, but in some cases (*e.g.* the NB; Fig. ~~13~~10) these units can be vertically and laterally closely associated and separated by the MES (e.g. Nijar Basin, Fig. ~~13~~10). However, in contrast with the PLG, the RLG base is commonly erosional. This is well represented in the BB section (Fig. ~~14~~11); here the RLG unit onlaps on the MES against the basin margin represented by a thrust-related anticline, whereas *in situ* PLG evaporites are truncated by the MES. RLG deposits may pass upslope to chaotic and/or irregularly bedded to transparent seismic facies with internal erosional surfaces. The Garrucha and Coscojar olistostromes of the Sorbas-Vera Basin (sector 3; see chapter 3.1.1.) may represent as well a good outcrop analog for some of the offshore chaotic units. Their expected seismic expression would be similar to the RLG of the Belice basin (Fig. ~~14~~11), with a chaotic and/or semi-transparent seismic facies showing an erosional base and an irregular top. As in the Belice~~B~~ b~~b~~asin (see Fig.

7b5b), the latter is not a subaerial unconformity, but an irregular, non-depositional and/or weakly erosional subaqueous surface draped by hemipelagic deposits.

The RLG interbedded clastic gypsum and mudstones are characterized in well logs by a typical spiky pattern (Fig. 7g5g), which is clearly distinguishable from the blocky pattern of the PLG evaporites. However, the large PLG olistoliths sitting within the RLG chaotic units could be interpreted as erosional remnants of *in situ* primary evaporites accumulated in a deep basin if crossed by a single borehole (e.g. BB, Figs 7g5g, 1411).

3.*3.3. MSC stage 3.* The seismic facies of stage 3 deposits (Table 34) are characterized by low to high-amplitude parallel reflectors due to the lithological contrast between gypsum or conglomerate/sandstone and marl/shale beds. They form tabular, "*bedded*" seismic units (BU) that may appear very similar to stage 1 PLG and stage 2 RLG units and that usually onlap the basin margins and the MES (see Sorbas and Nijar examples; Figs 129, 1310). The primary gypsum facies of shallow (Upper Gypsum – UG; Sicily, Cyprus) or intermediate depth (Tyrrhenian basin) may show gypsum/shale thickness ratios significantly lower than the PLG unit. As a consequence, the P-wave interval velocity of the BU-UG units may range between values as low as 2.2 up to > 4.0 km/sec (Fig. 9; Kastens et al., 1990). The absence of gypsum may hamper the distinction of stage 3 seismic units from the overlying Pliocene ones (Figs 129, 1310). Pliocene deposits usually consist of hemipelagic marls (*e.g.* Trubi Formationm.) and their base would display a strong lithological contrast only in places where the M/P boundary eventually corresponds to the topmost evaporite bed, a case that is not usually observed (see Fig. 8b6b). Deeper settings are locally characterized by the deposition of marls and turbiditic sandstones. Based on the results obtained for similar deposits (see stage 3 of Nijar Basin), their expected seismic expression is a "*bedded*" unit with low amplitude reflectors including slightly erosional surfaces forming flat cut-and-fill, channel-like features, as observed in the Cuevas del Almanzora section (Sorbas-Vera Basin; Fortuin et al., 1995; Figs ~~10c~~ 6~~7~~c,h ~~and 10h~~ ~~7h~~). The thickness of stage 3 deposits is highly variable; in intermediate depth/deep basins it can attain only a few tens of meters or even less (see the Vera and Belice basins). For this reason, these deposits can be commonly below the usual seismic resolution (~20-30 m) and hence not detectable in seismic profiles.

3.4 Seismic forward modelling - ~~Implications~~ implications for onshore-offshore correlations

In seismic profiles, the units of the three MSC stages (Table ~~1~~3~~2~~) result in regularly "*bedded*" (BU), chaotic and/or transparent (CU, MU) seismic units. These are differentiated on the basis of reflection~~or~~ amplitude, lateral continuity and thickness (Table ~~2~~4~~3~~) and on the erosional *vs.* non-erosional nature of their bounding surfaces (Fig. ~~2~~3, Table ~~3~~5~~4~~). However, synthetic seismic based on onshore data suggest that: 1) units with distinct palaeoenvironmental and chronostratigraphic meaning have very similar or even the same seismic facies ~~with none or very subtle differences~~; in fact, bedded seismic units with high-amplitude reflectors (BU) may correspond indistinctly to stage 1 PLG evaporites (BU-PLG), stage 2 RLG (BU-RLG) or stage 3 (BU-UG) deposits (Table ~~2~~3); 2) the same unit may show different seismic facies according to the dominant frequency and consequent vertical resolution. Nevertheless, our novel approach ~~- helps suggesting~~ provides some clues for establishing the possible nature of BU and CU units and tentatively assigning them to the corresponding MSC stages, on the basis of their bounding surfaces and of well logs patterns.

The three key surfaces ~~showing~~ with a strong chronostratigraphic meaning that may help in onshore-offshore and/or shallow-deep correlations are:

i) the base of the PLG evaporites of stage 1 (OS/EOS);

ii) the MES truncating the PLG unit and defining the transition between stage 1 and 2;

iii) the M/P boundary (Fig. ~~4~~2).

The PLG base (EOS) in offshore shallow-water would correspond to the Bottom Surface (BS); due to the apparent onlap of gypsum beds, this surface ~~it~~ could be wrongly interpreted as the Bottom Erosion Surface (BES; Fig. ~~12c~~9c, compare with Fig. ~~5c~~3c).

The PLG base (EOS) may develop diachronously; thus, the seismic expression of the OS is a high-amplitude reflector only in those shallow water settings (< 200 m) where it coincides with the EOS (Fig. ~~5b~~3b). Onshore the OS passes downbasin into a surface lacking any strong lithological contrast within shale deposits; thus, a weak reflector is expected. In intermediate to deep water basins evaporite-free, stage 1 deposits (*i.e.,* FBI organic-rich shales) are sharply overlain by the RLG unit; in this case the OS surface should be found *below* the BES/BS (Fig. ~~5d~~3d). The seismic expression of the FBI is expected to be a thin, tabular, almost transparent unit with very weak, parallel reflectors due to its homogeneous lithology. However, due to its reduced thickness (~~(~~< 50 meters; Manzi et al., 2007; 2018), ~~the~~ this unit could be seismically undetectable. In this case, for practical purposes, the BES/BS would be coincident with the OS, but this is a simplification that should be avoided as it may produce the erroneous correlation of seismically-similar deposits belonging to different MSC stages.

The erosional surface capping the BU-PLG (Fig. ~~5h~~3h,i) may correspond to the Top Erosion Surface (TES) or, in case they are overlain by stage 3 units (BU, UU), to the Intermediate Erosion Surface (IES). In any case, these surfaces can be traced downbasin into the BES and, more distally into the BS (Fig. ~~6~~4), at the base of the BU-RLG/UG (*i.e.*, LU-MU-UU) unit whose top, on the contrary, is usually conformable. Thus, the MES-TES-BES is a polygenic erosional surface with both subaerial and subaqueous tracts separating units with strongly similar seismic facies belonging to different MSC stages. Usually these units are detached and separated by intervening morphostructural elements; alternatively, they can be very tightly associated (Nijar Basin; Fortuin and Krijgsman, 2003; Omodeo-Salé et al., 2012; Fig. ~~13~~10), making their definition extremely difficult without tightly spaced cores.

Distinction between Stage 2 and 3 units cannot be based on lithology and seismic facies characteristics only. A straightforward correlation to stage 3 can be assigned only if samples are available from cores or cuttings and only when the primary gypsum (UG) or the typical Lagomare fossil assemblages (mollusk, ostracods, dinocysts) are recognized; an additional hint is provided by the gypsum or fossil $^{87}Sr/^{86}Sr$ values below 0.709088 (Roveri et al., 2014b). $^{87}Sr/^{86}Sr$ in halite shows values higher than those of stage 3 (Roveri et al., 2014b; Gvirtzman et al., 2017; Manzi et al., 2018); considering that halite occurs in a unit floored by the unconformity capping stage 1, the MU of intermediate depth basins may be a good potential marker for stage 2. However, the bedded units (BU, UU) above the MU not necessarily correspond to stage 3, because in onshore examples (Sicily and Calabria; Fig. ~~6a~~4a) halite bodies are commonly found encased within stage 2 clastic evaporites, both stratifed or chaotic. Significantly, stage 2 may include both the *"bedded"* units underlying (LU) and overlying (BU, UU) the MU. The latter situation has been well documented in the deep offshore basins, where the UU cored by DSDP-ODP drillings has been shown to include halite and anhydrite beds with stage 2 Sr isotope values (Roveri et al., 2014b); in most cases, only the topmost part of UU belongs to stage 3 (Roveri et al., 2014b).

A similar problem can be envisaged for the surface(s) marking the end of the salinity crisis; onshore the M/P boundary is locally characterized by strong lithological contrasts corresponding to flooding and/or ravinement surfaces (the latter having a slight erosional character; Fig. ~~8c~~6c-f); in deeper settings and offshore, the top of the MSC units is labeled as Top Surface (TS) or TES. However, it has been shown (Roveri et al., 2014b) that these surfaces may actually correspond to the top of uppermost evaporitic deposit, which is not necessarily coincident with the M/P boundary (see Fig. ~~8b~~6b) and may belong to stage 2 or to stage 3. In deep basinal settings a thin evaporite-free unit, commonly below seismic resolution and belonging to stage 3, can occur between the uppermost evaporite and the M/P boundary (Roveri et al., 2014b; Gvirtzman et al., 2017). As a consequence, the correspondence of the TS/TES with the end of the crisis could be only apparent and related to the seismic resolution.

Defining the nature of offshore MSC surfaces and units is not an easy task as no univocal correspondence with onshore units exists, with obvious implications for a correct reconstruction of the Messinian stratigraphy and events. Our analyses show that seismic facies alone are not decisive for defining the nature and stratigraphic position of a specific MSC unit or surface and even sparse cores could be not sufficient to solve the problem in areas with strongly articulated successions. As a consequence, a word of caution is needed when deriving general implications from offshore MSC record.

4. REVISITING THE MSC RECORD OF THE BALEARIC PROMONTORY

4.1 - The MSC record of the Balearic Promontory: state of the art

The results and the insights of our approach, let us ~~to~~ propose a revisitation of the Messinian stratigraphic architecture of the offshore Balearic Promontory ~~(BP)~~, a narrow morphostructural high bounded to the north and to the south by the deep Valencia and Algero-Balearic basins (Fig. ~~15a~~12a), representing the northeastward extension of the Betic Cordillera ~~(BC(;~~ Fig. ~~15a~~12a; Etheve et al., 2016). As the Betic Cordillera, the Balearic Promontory ~~area~~ underwent compression during the Langhian-Serravallian (Sanz de Galdeano, 1990) and extension since the Late Miocene (Fig. ~~15b~~12b). This caused the observed complex morphology with depressions at different water depths (Fig. ~~15b~~12b) that acted as perched sub-basins, as shown by the onlap against the intervening structural highs (Martinez del Olmo, 2011a-b; Maillard et al., 2014; Driussi et al., 2015). The deepest bathymetric low is the Central Mallorca Depression (~~CMD; ~~Fig. ~~15b~~12b).

The MSC seismic units of the Balearic Promontory are physically disconnected and are mainly characterized by parallel, high-amplitude reflectors (see Driussi et al., 2015, their figures ~~Figs~~ 7,8,11). Due to the poor development or absence of the Mobile Unit (MU), the successions are not tripartite and these "*bedded*" units that could correspond either to the Lower Unit (LU) or Upper Unit (UU) have been labeled as a chronostratigraphically unconstrained Bedded Unit (BU) (Maillard et al., 2014; Driussi et al., 2015). A halite-bearing unit possibly occurs in the ~~CMD~~ Central Mallorca Depression below a BU (Maillard et al., 2014; Driussi et al., 2015); both units onlap against an erosional surface, more clearly at the eastern margin. Here, a Slope Unit (SU) consisting of both chaotic and bedded seismic facies bounded by erosional surfaces has been identified (Maillard et al., 2014, their figures 5 and 6c). Further upslope, a *"bedded"* unit with erosional top has been observed on the Mallorca shelf. This unit, cored in the Palma de Mallorca borehole (Rosell et al., 1998; Fig. ~~15c~~12c), consists of *in situ*, selenite gypsum beds showing the typical PLG well log blocky pattern (Fig. ~~5a~~3a; Roveri et al., 2008b; Lugli et al., 2010; Roveri et al., 2014a). Due to the similar number of cycles (13) and stacking pattern, a correlation with the PLG outcropping in the Sorbas basin and drilled in the Bajo Segura basin (La Mata, San Miguel-2, Benejuzar-1, Rojales-1, La Marina-1 boreholes) has been suggested (Rosell et al., 1998; Soria et al., 2008; Martinez del Olmo, 2011a,b; Corbì et al., 2016; Figs S1d, ~~14d~~121d, ~~15b~~12b). Martinez del Olmo (2011b) proposed the same correlation for the evaporites drilled offshore (Muchamiel, Calpe-1, Golfo de Valencia-1 and Castellon-L1 boreholes), indicating that the distribution of gypsum is limited to the more marginal areas (see Fig. ~~15d~~12d). The 497-Muchamiel and 334-Calpe 1 boreholes are located on the shelf (location in Fig. ~~14b~~12~~1~~b) and confirm the presence of the PLG unit in the Elche sub-basin (Fig. ~~15b~~12b; Martinez del Olmo, 2011b; Ochoa et al., 2015), at present-day depths ranging between 600 and 900 m below the mean sea-level. The PLG have also been found basinward of an inferred Messinian shelf-edge (Maillard et al., 2014; Fig. ~~15c~~12c; their figures 3 and 11; Driussi et al., 2015). In the Mallorca island (Fig. ~~15c~~12c) these evaporites pass landward to shallow water microbial carbonates (TCC, Terminal Carbonate Complex) resting on top of pre-evaporitic reefs (Arenas and Pomar, 2010; Mas and Fornos, 2012; Mas, 2015). The TCC deposits are capped by a well-developed reddish paleosol (Mas, 2015), suggesting a prolonged subaerial exposure, and unconformably overlain by a thin marly unit with uppermost Messinian Lago-Mare faunal assemblages. The Lago-Mare unit, in turn, is sharply overlain by Pliocene calcarenites, possibly recording the Zanclean marine flooding (Mas and Fornos, 2012; Mas, 2015). The PLG evaporites also occur in the offshore portion of the Bajo Segura basin, where they apparently onlap the slope of a lower Messinian reef drilled by the Torrevieja Marino 1 well (Martinez del Olmo, 2011a) whose top is at 650 m below sea-levl (bsl, Fig. ~~15d~~12d-f).

The MSC evaporites also occur in the deepest sectors of the BP area including the Cogedor, Formentera and Central Mallorca Depression sub-basins (Fig. 15b; Maillard et al., 2014; Driussi et al., 2015; Ochoa et al., 2015). These sub-basins, separated by acoustic basement highs, contain a *"bedded"* seismic unit, similar to the BU-PLG of the Elche sub-basin, but clearly distinct from it (see figure 2 of Ochoa et al., 2015) and labeled as chronostratigraphically unconstrained BU (Driussi et al., 2015). Despite these uncertainties, Ochoa et al. (2015) argued that this unit could be coeval and perfectly equivalent of the BU-PLG, thus suggesting that PLG evaporites were deposited also in deeper and not silled areas, differently to what envisaged by the PLG model of Lugli et al. (2010).

4.2 – The MSC record of the Balearic Promontory: an alternative view

The distribution pattern of the Messinian deposits and the small size of the BP sub-basins, separated by tectonic and volcanic highs (Maillard et al., 2014; Driussi et al., 2015), closely resembles the onshore basins of many peri-Mediterranean areas (Fig. ~~10~~7). All these basins document extremely rapid facies and stratigraphic changes controlled by topography (Roveri et al., 2003; Omodeo-Salé et al, 2012) and thus can be a good analog of the BP.

The evaporites identified in the Elche and San Pedro sub-basins and in the area of Palma de Mallorca (Fig. ~~15b~~12b) formed beyond a Messinian shelf edge. The seismic and borehole data of the Bajo Segura-San Pedro basin (Martinez del Olmo, 2011a) clearly document the offshore continuation of the evaporites of San Miguel de Salinas and their onlap against the Torrevieja Marine C-1 Messinian reef (Figs ~~15e~~12e-f). $^{87}Sr/^{86}Sr$ (Fig. S14) ~~(Fig. 16a)~~ measured in gypsum samples from San Miguel de Salinas and Benejuzar outcrop sections (Fig. ~~16b~~S14b,c) show values typical of the first stage PLG evaporites (Fig. ~~16d~~S14d-e; Roveri et al., 2014b). Cuttings from the Torrevieja M. C-1 well consist of *Porites*, stromatolitic and oolitic limestones, suggesting that the reef can be correlated with the outcropping Santa Pola, Cariatiz, and Palma reefs. The reef top lies today at ~620 mbsl, while gypsum is found at a depth of ~800 m (Martinez del Olmo, 2011a); the difference in elevation (~200 m; Fig. 15f) is comparable to that estimated in the Sorbas basin (~240 m; Riding et al., 1998; Fig. 12).

As a consequence, the situation in the Balearic Promontory is similar to what is observed in the Betic Cordillera basins, where the PLG evaporites formed *basinward* with respect to the outermost pre-MSC reef front (see synthetic seismic profile of the Sorbas basin in Fig. ~~12~~9), but still at relatively shallow depths and in silled sub-basins.

The seismic profile SIMBAD BA-26 (S26 in Fig. ~~17~~13a,b; Driussi et al., 2015) shows that toward the southeast the BU-PLG unit disappears over an eroded basement ridge (the Elche high) crossing the Elche sub-basin; this ridge seems to represent the north-east extension of a narrow, evaporite-free belt corresponding to the Tabarca-Alicante basement high (Fig. ~~17a~~13a). The same seismic profile shows a deeper sub-basin beyond the Elche high, characterized by a bedded seismic unit (BU) showing: i) a basal unconformity (Fig. ~~17b~~13b~~-c~~), ii) clear onlap terminations against the basement and/or pre-Messinian units, and iii) a lateral facies change from bedded to chaotic deposits (CU; Fig. ~~17c~~13c). Onlap terminations do not characterize only the Messinian units but also the pre-MSC and the Pliocene units, thus suggesting that these basement ridges were active before, during and after the crisis, creating a strongly articulated topography.

In our view, also based on a comparison~~s of seismic units and reflectors geometries between~~of profile S26 (Fig. 13a,b) ~~and~~with the synthetic sections of Nijar and Belice basins (Figs 10, 11), the Elche sub-basin can be subdivided into two sectors (Fig. ~~17a~~13a): 1) a southeastern, deeper sector with the generic BU unit also observed in the Cogedor, Formentera and Central Mallorca Depression sub-basins (Maillard et al., 2014), 2) a northwestern, shallower one showing the BU-PLG unit. ~~Although~~In fact, both the~~,~~ Nijar and Belice basins ~~have a different Messinian stratigraphy, the~~show narrow erosional areas (corresponding to structural highs) separating shallower and deeper sub-basins ~~generate~~with Messinian ~~seismic~~units having apparently the same seismic ~~features~~characteristics but very different environmental and stratigraphic meaning (*i.e.*, respectively, the BU-PLG and a generic BU), ~~similar to those~~a situation that may well apply to -what observed in ~~of~~ the Elche basin ~~(*i.e.*, BU-PLG and generic BU)~~.

Seismic profiles MED 5B (crossing S26 at its SE end) and MAP 146 (figure 3 of Ochoa et al., 2015; see location in Fig. ~~17a~~13a) run across the southeastern sector of the Elche sub-basin but not in the northwestern one (Fig. ~~17a~~13a). The areas separating the shallower and deeper sub-basins include chaotic units bounded by erosional surfaces. As a consequence, in contrast to Ochoa et al. (2015), we argue that no lateral transition from the BU-PLG unit of the Elche sub-basin to the BU unit of the Formentera sub-basin can be documented. In facts, the two sub-basins were separated by a pre-existing intrabasinal high and the two units show well distinct features. The BU-PLG of the inner, shallower and the BU of the outer, deeper sub-basins appear to be neither physically nor genetically connected and are instead separated in time and space by an unconformity truncating the first and underlying the second one. The deeper BU is here interpreted as BU-RLG, possibly recording stages 2 and 3 (Fig. ~~17~~13b).

As for the end of the MSC, seismic and borehole data do not have the resolution needed to fully constrain it. In the Muchamiel and Calpe boreholes the PLG are unconformably overlain by early Zanclean micritic limestone, but the occurrence of thin uppermost Messinian deposits between the erosional surface and the Pliocene limestones is not ruled out (Ochoa et al., 2015). This is the case of the Mallorca island where a very thin (5 m) Lago-Mare unit is present below the Pliocene deposits; this transition is considered unconformable by some authors (Mas and Fornos, 2012; Mas, 2015) and associated with the main Mediterranean drawdown. Such a thin unit cannot be distinguished on seismic profiles and could be even below the sampling resolution of well cuttings.

4.3 - A three stages record of the MSC in the Balearic Promontory

The Bedded Unit-Primary Lower Gypsum (BU-PLG) of the shallower areas and the BU and SU of the deeper settings of the Balearic Promontory can be framed within the MSC three-stage scenario (CIESM, 2008; Roveri et al., 2014a; Fig. 18). These seismic units may record ~~respectively~~ the first and second stage, respectively, forming distinct units separated in time by an erosional surface and arranged in different, commonly disconnected, depocenters. The upper part of the BU unit, particularly where it is topped by the TS, may record the third stage. As previously mentioned, in the onshore basins stage 3 deposits are mainly composed of well-layered clastic sediments (but locally including the UG in Sicily, Cyprus and Crete; see synthetic seismic of Figs ~~12~~ 10 and ~~13~~11).

In our view, during the Messinian the Balearic Promontory was a marginal basin with both shallow and intermediate depth perched and semi-closed sub-basins with different stratigraphy (Fig. ~~18~~13C~~14~~), similar to the situation shown in our synthetic seismic sections of the Nijar and Belice basins (Figs. 10, 11). PLG evaporites accumulated only in the shallower sectors of the Elche, San Pedro and Mallorca sub-basins. These sub-basins were semi-closed, bounded by carbonate platforms and separated by volcanic/structural sills from deeper areas and exposed to subaerial erosion after the stage 1. After or during the phase of erosion, that affected the basin margins of the entire Mediterranean, a halite-bearing bedded unit floored by the MES developed in deeper sub-basins (Central Mallorca Depression, Formentera, Cogedor, Elche deeper sector). It follows that the MES actually separates units deposited in different times and in different depocenters at variable original water depths. These depocenters were separated by morphostructural highs (basement, volcanic/structural) characterized by erosion/non-deposition of MSC units or by the emplacement of chaotic deposits (SU) showing complex lateral facies changes and stratigraphic relationships with the BU units (see the Nijar and Belice examples; Figs ~~13~~ 10 and ~~14~~11). In our view, they mainly formed during stage 2 (see Fig.

~~18c~~13C~~14c~~). Thus, the MES developed on top of the BU-PLG unit passes downslope into a BES underlying the SU and BU (Fig. ~~18~~13C~~14~~). The latter may locally include halite bodies accumulated in closed depressions, independently of their absolute water depth, as observed in other Mediterranean areas (Sicily, Tuscany, Calabria, Cyprus; Roveri et al., 2014a).

5. IMPLICATIONS FOR THE WIDER MEDITERRANEAN~~-SCALE IMPLICATIONS~~

The implications recently derived from the BP Messinian record (Maillard et al., 2014; Ochoa et al., 2015) may be very important at a Mediterranean-scale and for this reason need to be carefully evaluated and discussed on the light of our results.

5.1. MSC onset *vs.* evaporite onset

Ochoa et al. (2015) stated that the onset of evaporite deposition occurred synchronously throughout the shallow to deep Mediterranean settings and in coincidence with the onset of the MSC. Conversely, we showed that the Balearic Promontory underwent strong subsidence in post-MSC times and that during the Messinian it was a shallow-water basin, perfectly correspondent to the depositional settings where all the known examples of PLG evaporites formed. Moreover, onshore-based studies demonstrate that the concept of MSC onset should be kept well separated from the simplistic identification of the “first gypsum bed” (Fig. ~~5a~~3a). Borehole data alone, without continuous cores or closely spaced cuttings, do not have the necessary resolution to prove or disprove this interpretation. In facts, considering the reduced sedimentation rate of the pre-MSC and FBI (commonly < 100 mm/kyr; see Fig. S2 of Manzi et al., 2018), the adequate sampling resolution to obtain a reliable stratigraphic framework would range from 2-3 m to 1 m or less.

5.2 PLG basins: silled *vs.* open, shallow *vs.* deep

Ochoa et al. (2015) suggest that the PLG evaporites were not limited to shallow-water silled basins, but also precipitated *beyond* the Messinian shelf break along the continental margin slopes in open and deep settings.

In our alternative reconstruction of the Messinian stratigraphy of the Balearic Promontory, the PLG units were deposited only in the inner sector, where they onlap against pre-evaporitic reefs and are truncated by an erosional surface; this sector is bounded basinward by several aligned morphostructural highs that were already present during the Messinian and likely acted as sills. In this sector the PLG evaporites currently lie at a depth of 800-900 m bsl, and the top of pre-MSC reef (that can be considered a good shoreline marker) at 630 m bsl. The difference in elevation suggest that the PLG evaporites started to accumulate in silled sub-basins at around 200 m water-depth, perfectly similar to the Sorbas-Vera Basin example (see chapter 3.1.1). Far from being at intermediate water depth (200-1000 m) during the MSC, this shallow-water area underwent considerable subsidence in post-Messinian times. The deeper sector beyond the structural highs is characterized by deposits more similar to those of stages 2 and 3. It results that the PLG distribution in the Balearic Promontory is perfectly comparable to that observed onshore, thus supporting the Lugli et al.'s (2010) model.

5.3 Halite deposition: shallow or deep, synchronous or diachronous?

The occurrence of the halite bodies in relatively small onshore basins of Sicily, Tuscany, Calabria and Cyprus, demonstrate that these deposits did not necessarily form in the deepest Mediterranean basins, usually floored by oceanic or thinned continental crust, but also at shallower depths.

In order to explain the occurrence of the thin MU in the CMD, fully detached from the main deep basin salt unit and formed at intermediate depths, Maillard et al. (2014) argued that either the Mediterranean sea-level drop was not so large or the salt was deposited diachronously at different depths during the evaporative drawdown.

We suggest a third hypothesis: the accumulation of halite was not dependent on water depth but only on the existence of brine traps in confined sub-basins. Closed or semi-closed depressions occurring at any depths may have trapped brines formed in shallow-water settings and transferred at depths by cascading currents (Roveri et al., 2014c).

6. CONCLUSIONS

Our findings suggest that:

1. synthetic seismic profiles of onshore sections can be a very helpful tool allowing ~~to compare~~ onshore and offshore MSC records to be compared;
2. lacking core data, the nature and the stratigraphic position of the offshore BU and transparent units cannot be univocally defined on the base of seismic data only;
3. rapid lateral thickness variation and the strong acoustic impedance contrasts with interbedded, underlying or lateral equivalent deposits may result into misleading geometries of evaporite-bearing units, simulating false angular discordances and/or onlap terminations;
4. out of the three main MSC surfaces defined onshore and marking the onset (OS), the end (M/P) and the peak of the crisis (MES) at stage 1-2 transition, only the latter can be unambiguously recognized offshore; it corresponds in shallow areas to the TES/IES and can be traced downbasin into the BES/BS surface;
5. in intermediate depth and deep settings, the OS and the M/P commonly occur within evaporite-free units characterized by weak seismic images and may be not recognized;

6. the commonly assumed correspondences OS = BES/BS and M/P = TES/TS in the interpretation of the deep succession are not necessarily correct;
7. the Balearic Promontory underwent strong post-MSC subsidence, but both shallow and intermediate depth sub-basins settings were present during the salinity crisis;
8. a three-stage MSC scenario also applies for the Balearic Promontory; primary *in situ* evaporites of stage 1 occur only in the shallower silled sub-basins of the Balearic Promontory, in agreement with the model of Lugli et al. (2010); generic BU units of deeper sub-basins show an erosional base that can be traced into the erosional top surface of BU-PLG, suggesting their formation during stage 2;
9. Slope (SU)~~U~~ and Complex (CU) units may correspond, at least partially, to chaotic deposits emplaced by gravity flows; the Garrucha-Coscojar olistostrome of the Sorbas-Vera basin and those of the Sicilian basins, all containing small to giant PLG gypsum blocks, may be a good outcrop analogue; SU may also consist of carbonate, hybrid or siliciclastic ramp deposits, that are locally developed and preserved along Messinian basin margins;
10. the occurrence of halite bodies in perched basins at different water depths can be explained by the trapping of brines cascading from shallow-water settings into semi-closed basins, thus not implying the desiccation and/or high-amplitude oscillations of the Mediterranean sea-level.

Summarizing, our results show that a word of caution is needed in reconstructing Messinian stratigraphy only from seismic data, as the Messinian events resulted in a complex framework with tight relationships between units having similar geometries, bounding surfaces and lithological characteristics and hence similar seismic response, but that may belong to different stages and have completely different meanings.

ACKNOWLEDGMENTS

Clara Rodriguez and Rebecca Bell are gratefully acknowledged for their constructive comments, that significantly improved this manuscript. UNIPR and UNIMORE research funds covered costs of Sr isotope analysis. We thank A. Cipriani for facilitating these analyses at the UNIMORE laboratory. This is ISMAR-CNR, Bologna, scientific contribution n. 1986.

FIGURE CAPTIONS

Fig. 1 – Distribution of Mediterranean sub-basins during the late Messinian (modified after Roveri et al., 2014a). Marginal/peripheral sub-basins include both shallow-water (0–200 m) and intermediate depth settings (200–1000 m), while deep sub-basins (>1000 m) are present only in the central domain.

Fig. 2 – Present-day distribution of the Messinian basins; compare with figure 1. Note that marginal/peripheral basins with shallow and intermediate depth sub-basins occur both in onshore and offshore areas, according to post-Messinian tectonic evolution. For deep central basins both Western and Eastern Mediterranean markers are shown (from Lofi et al., 2011a,b).

Fig. 3 1 – Tentative onshore-offshore correlation of the Messinian units and surfaces (modified from Roveri et al., 2014b).

Fig. 4 2 – Conceptual stratigraphic model of the Messinian deposits of shallow and intermediate depth sub-basins. PLG = Primary Lower Gypsum; FBI = foraminifer-barren unit; RLG = Resedimented Lower Gypsum; UG = Upper Gypsum; MES = Messinian erosional surface; MES-cc =

correlative conformity; M/P = Messinian-Pliocene boundary; OS = onset surface of the Messinian salinity crisis; EOS = evaporite onset surface; TCC = Terminal Carbonate Complex.

Fig. ~~5~~ 3 – Stage 1 deposits and surfaces: outcrop examples. Black labels refer to the possible corresponding offshore markers (see chapter 3.4); A) the Primary Lower Gypsum (PLG) cycle model and the stacking pattern of PLG unit in outcrop and borehole sections; note the thinner basal cycles (1-2), the thicker cluster of cycles 3-4-5, the facies change at cycle 6 and the typical blocky pattern in well logs; Elsa 1 well shows a top-missing PLG record (due to erosion); in the Pollenzo section (see D) onset of evaporite deposition is delayed; in this case the onset of evaporites (EOS) is not coincident with the onset of the salinity crisis (OS). *Bottom surfaces* - B) Monticino section (Northern Apennines, Italy): base of PLG unit (BS) with the two lowermost thinner cycles; MSC onset and evaporite onset are coincident; C) Perales section (Sorbas basin, Southern Spain): laterally discontinuous gypsum lenses within PLG cycle 1, resulting in the local coincidence of OS and EOS surfaces (BS/BES); D) the Pollenzo section shown in A): white lines corresponds to the base of precessional cycles within the FBI unit and corresponding to PLG cycles 1 to 4; PLG onset (BS) occurred only at cycle 5. *Internal surfaces* **-** E) San Miguel de Salinas section (Bajo Segura basin, Spain) and F) Rio Aguas section (Sorbas Basin, Southern Spain): irregular top surface and abrupt lateral closures of gypsum beds due to the depositional geometry of growing selenite gypsum simulating erosional features (IES or TES); note the contrast between the flat basal and the irregular top surfaces of individual gypsum beds; G) Barranco de Infierno (Sorbas Basin, Southern Spain): upper part of the Yesares Mb. showing the lenticular geometry of uppermost gypsum beds passing laterally to limestone and marls (IES or TES). *Top surfaces* **-** H) Monticino section (Northern Apennines, Italy) and I) Krystal Beach section (Zakynthos, Greece): the subaerial erosional surface (MES) developed on top of the tilted PLG unit sealed by uppermost stage 3 (Lago-Mare) and Zanclean open marine deposits.

Fig. ~~6~~ 4 – Stage 2 deposits and surfaces: outcrop examples. Black labels refer to the possible corresponding offshore markers (see chapter 3.4); A) T. Lepre section (Crotone basin, Calabria, Italy); here the MES partially erodes the MSC stage 1 FBI unit; the RLG unit consists of clastic gypsum enclosing small halite bodies; B) Fanantello section (Northern Apennines, Italy) showing the FBI sharply overlain by RLG deposits consisting of a basal stratified gypsarenite unit, in turn overlain by chaotic deposits with gypsum olistoliths; C) simplified geological map and cross-section of Sicily (from Roveri et al., 2008); D) Sutera (Caltanissetta basin, Sicily); the village lies at the base of a huge PLG block floating on a chaotic mudstone matrix including olistoliths of gypsarenites and diatomites, resting upon pre-MSC deposits; E) Ciminna basin (Sicily); horizontally stratified RLG gypsarenites and gypsrudites onlapping tilted PLG blocks and overlain by a second unit made of PLG slide blocks (from Roveri et al., 2008); F) Balza Bovolito (Petralia basin, Sicily); RLG stratified gypsarenites passing upward to stratified calcirudites and calcarenites; these deposits onlap and/or pass laterally to chaotic deposits and massive limestone breccia (modified from Manzi et al., 2011); G) Garrucha olistostrome (Sorbas-Vera basin, Spain; location in Fig. 7b,c)); gypsarenite and gypsrudite beds with gypsum olistoliths in the Garrucha olistostrome; H) PLG block, not *in situ*, included in the Garrucha-Coscojar olistostrome; I) large recrystallized PLG block in the Coscojar olistostrome (Sorbas-Vera basin, Spain; location in Fig. 7b).~~.~~

Fig. ~~7~~ 5 – Stage 2 deposits and surfaces: outcrop examples. Black labels refer to the possible corresponding offshore markers (see chapter 3.4); A) Passo Fonnuto (Caltanissetta basin, Sicily);

onlap of uppermost UG and Pliocene deposits against PLG slide blocks floating on top of a chaotic unit; ~1 km to the right a halite body is present under the river alluvional cover; B) Belice basin (Sicily); PLG blocks in a chaotic matrix directly overlain by lower Pliocene Trubi; C) nearby Racalmuto (Caltanissetta basin, Sicily); the RLG unit consists here of a basal chaotic body with large PLG blocks embedded in a mudstone matrix; stratified gypsarenites and gypsrudites onlap the PLG blocks; D) Santa Ninfa (Belice basin, Sicily); panoramic view showing the relationships between the stratified gypsum turbidites and the overlying chaotic deposits including large size PLG blocks and the pre-evaporitic unit; note the onlap of turbidites against a small lower Messinian *Porites* reef; E) Rocca delle Penne (Belice basin, Sicily); a giant PLG olistolith floating within a chaotic mass consisting of disarticulated and chaotic shales, gypsarenites, gypsrudites and marls; note the size of the olistolith which in this case includes the three basal cycles simulating a *in situ* PLG unit; the bottom and top surfaces of this body, if imaged in seismic profiles and/or crossed by boreholes, could be interpreted as BS/BES and TES, respectively ; F) Belice basin (Sicily), close to E), a chaotic unit with PLG blocks sandwiched by gypsum turbidites forming a tabular, stratified unit (compare with synthetic section of Fig. 14); G) the typical spiky well log facies of RLG deposits; the figure also shows the possible close association with a PLG block.

Fig. ~~8~~ 6 – Stage 3 deposits and surfaces: outcrop examples. Black labels refer to the possible corresponding offshore markers (see chapter 3.4); A) Eraclea Minoa section (Sicily); irregular top of the 6th gypsum bed in the Upper Gypsum unit due to the domal growth geometry of gypsum crystals (IES/TES); B) location as A); the M/P boundary (corresponding to the Zanclean GSSP) occurs slightly above the irregular top of the topmost, 7th, UG bed; TS/TES is not coincident with the end of MSC; notice the presence of terrigenous fluvio-deltaic deposits in light green and orange in both the pictures; C) Nijar basin (Southern Spain); the cyclic stacking pattern of fluvio-deltaic and lacustrine deposits of MSC stage 3 Feos Fm.; strong reflectors are expected at the sharp transition from conglomerates to basinal marls; D) same location of C); transition to marine Pliocene deposits in the Los Castellones section; the Pliocene transgression in the Zorreras E) and la Cumbre F) sections (Sorbas basin); G) the organic-rich black layer marking the Miocene-Pliocene boundary in the Northern Apennines (Italy); H) Zanclean marls with thin-bedded turbidites in the Cuevas del Almanzora section (Vera basin); note the lenticular geometry of sandstone beds and the cut and fill structures, resulting in minor erosional surfaces.

~~Fig. 9 – Offshore example of stage 2 and 3 deposits from the Tyrrhenian basin and their tentative correlation with onshore RLG and UG deposits of the Caltanissetta basin (Sicily; modified from Roveri et al., 2014b and Manzi et al., 2009). In this case, the observed BU unit consists of thin both primary (cumulate) and clastic (gypsarenites and gypsrudites) gypsum beds interbedded with thick marls; as a consequence, the P-wave interval velocity of this evaporite-bearing unit is relatively low (~2.3 km/sec.). The UG deposits can be easily distinguished from the RLG and pre-MSC deposits due to a distinctive isotopic signature.~~

Fig. ~~10~~ 7 – Schematic geological map of Southern Spain (A) with location of the Sorbas-Vera (B) and Nijar sub-basins (Fig. ~~13~~10). (C) cross section showing that the Garrucha body was emplaced in an erosional depression cut in the underlying pre-MSC tilted succession (modified after Fortuin et al., 1995; Di Blasi, 2018); (D) Cross-section along the Sorbas-Vera basin. Notice the sill and the narrow, steep slope separating the shallow Sorbas sub-basin (Sector 1) and the deeper Vera sub-basin (Sector 4). The Sorbas-Vera corridor is here interpreted as a possible Messinian canyon showing an upper erosional tract (Sector 2) and a lower one with chaotic deposits (Sector

3; Garrucha olistostrome in the area shown in Fig. ~~11a~~8a,b); turbiditic lobes are developed in the slope base area and in the Vera sub-basin (Sector 4) .

Fig. 8 – Stratigraphic logs and seismic wavelets used for the reconstruction of the synthetic seismic sections of the Sorbas (a), Nijar (b) and Belice (c) basins; the logs are shown in real depth and after transformation in time domain through the seismic parameters listed in Table 2. For each log in time domain, the resulting wavelets at 60 and 180 Hz are shown.

~~Fig. 11 8 – Strontium isotope data ($^{87}Sr/^{86}Sr$) from selenite gypsum of tThe Garrucha-Coscojar area of the Sorbas-Vera basin; A) Simplified geological map (see location in Fig. 107) showing the location of the gypsum-bearing Coscojar and Garrucha olistostromes and of of analyzed samples for Sr isotope analysis (see Fig. S4); the B) cross section showings that the Garrucha body was emplaced in an erosional depression cut in the underlying pre-MSC tilted succession (modified after Fortuin et al., 1995; Di Blasi, 2018); BC) PLG block, not *in situ*, included in the Garrucha-Coscojar olistostrome; C) table with the $^{87}Sr/^{86}Sr$ values; the values fall in the range of the first stage of the salinity crisis; D) gypsum selenite clasts within a laminated gypsarenite; E) detail of a gypsum clast containing microbial filaments from the outcrop shown in B); F) gypsarenite and gypsrudite beds with gypsum olistoliths in the Garrucha olistostrome; G) large recrystallized PLG block in the Coscojar olistostrome.~~

Fig. ~~12~~ 9 – Sorbas basin synthetic seismic section (see also Fig. 8a~~S1~~); A) geological cross-section in depth domain (see location and legend in Fig. ~~10b~~7b; modified from Roveri et al., 2009) with the location of the hypothetical boreholes used for the reconstruction of synthetic seismic section; B-C) the synthetic seismic section in time domain with different dominant frequency: 60 Hz (B) and 180 Hz (C) resulting in different seismic resolution; black labels show the possible offshore units (white) and surfaces (yellow). In (D-I) a close-up of the PLG unit is shown with different seismic resolution; it is worth noting how the seismic aspect is function of the adopted frequency. At low frequencies of 40 and 60 Hz (D-E) the PLG appears as a chaotic/transparent unit. Starting from 120 Hz (F) PLG appears as a bedded unit (BU) only in its basal part; for a full resolution, higher frequencies between 180 (G) and 250 Hz (H) are needed; at 500 Hz (I) even the thinner beds are visible. In (F-I) a transparent unit in the lower part of the BU-PLG unit corresponds to the thickest PLG cycle 3; its lateral pinchout results in an apparent discordance; in this case both the PLG base and the top of cycle 3 could be erroneously interpreted as unconformities (BES and IES, respectively).

Fig. ~~13~~ 10 – Nijar basin synthetic seismic section (see also Fig. 8b~~S2~~); schematic geological map (A) and cross-section in depth domain (B) of the Nijar basin (modified from Omodeo Salé et al., 2012; see location in Fig. ~~10b~~7b) with the location of the hypotethical boreholes used for the reconstruction of synthetic seismic section. C-D) the synthetic seismic section in time domain with different dominant frequency: 60 Hz (C) and 180 Hz (D) resulting in different seismic resolution; black labels show the possible offshore units (white) and surfaces (yellow). Note the complex stratigraphic architecture of the Messinian succession resulting in very close relationships between bedded and chaotic units belonging to the three MSC stages; note in the enlarged area shown at different dominant frequencies (from 40 Hz to 500 Hz) that, without direct observations or borehole data, the BS (placed at the base of *in situ* PLG deposits) would be cut by an internal erosional surface (IES) passing downslope to the BES; IES and BES would actually represent the downbasin equivalent of the MES, separating MSC stage 1 and 2. At least three BU units can be defined: 1) BU-PLG capped by the MES/IES; 2) BU-RLG within the erosional depression (possibly a canyon or gully head); 3) BU corresponding to stage 3 (=UU, but evaporite-free); at low frequency (40 to 60 Hz) the upper unit shows a seismic facies transparent or with discontinuous reflectors, simulating a chaotic deposit.

Fig. ~~14~~ 11 – Belice synthetic seismic section (see also Fig. 8c~~S3~~); A) cross-section in depth domain of the Belice basin (modified from Roveri et al., 2006; see location in Fig. ~~6c~~4c;); note PLG deposits on top of a thrust-related anticline cut by the MES and resedimented evaporites in the adjoining, deeper sub-basin, forming a complex RLG unit; note also the pre-MSC reef in the deeper basin which underwent strong tectonic subsidence during the Messinian; B–C) the synthetic seismic section in time domain with different dominant frequency: 60 Hz (B) and 180 Hz (C) resulting in different seismic resolution; black labels show the possible offshore units (white) and surfaces (yellow). Note the onlap of BU against the basal surface and an internal surface, the latter marking the top of a chaotic body; BU units in the deeper basin correspond to gypsum turbidites of MSC stage 2; the irregular top of the upper chaotic body could be exchanged for an erosional surface and, due to the very thin Lagomare deposits above it, it could apparently be coincident with the M/P boundary and labeled as TES. Note also the large PLG olistoliths within the chaotic units (compare with photo in Figs ~~6~~4-5~~7~~).

Fig. ~~15~~ 12 – Messinian units in the Balearic Promontory area; A) schematic tectonic map of the Western Mediterranean showing the location of the Balearic Promontory; B) present-day distribution of the Messinian units in the Balearic Promontory and adjacent areas (from Ochoa et al., 2015); 334 = Calpe 1 well; 497 = Muchamiel well; MCD = Mallorca Central Depression; BP = Balearic Promontory; CMD = Central Mallorca Depression; PLG = Primary Lower Gypsum unit; note the distribution of inferred PLG deposits in the Elche sub-basin and compare with Fig. 16a; C) location of the PLG evaporites of the Palma sub-basin (from figure 11 of Maillard et al., 2014);

the units were deposited in a narrow basin delimited by structural highs and bordered by Messinian reefs; the comparison with B) documents the similarities with the Sorbas Basin in terms of size and overall stratigraphic architecture; D) the distribution of PLG evaporites in the Balearic Promontory and Valencia Basin according to Martinez Del Olmo (2011); E) the Torrevieja Marino Messinian reef (see location in D); contour lines refer to the elevation of reef deposits above the highest onlap of PLG evaporites; seismic lines across the reef (F) show the 360° onlap of PLG evaporites against the reef front; difference in elevation between the reef top and the gypsum suggest an original paleodepth of around 200 m.

~~Fig. 16 – Strontium isotope data ($^{87}Sr/^{86}Sr$) from selenite gypsum of the onshore successions of Benejuzar and San Miguel de Salinas; the values fall in the range of the first stage of the salinity crisis. A – table with the $^{87}Sr/^{86}Sr$ values; B – simplified geological map of the Bajo Segura basin with the location of the main outcrop sections and boreholes crossing the PLG deposits; C - Sedimentary logs of the Benejuzar and San Miguel de Salinas sections showing the location of samples for Sr isotope analysis; D – Strontium isotope values framed in the Messinian Sr isotope stratigraphy; E –stratigraphic framework of the MSC (modified from Manzi et al., 2013 and Roveri et al., 2014a).~~

Fig. ~~17~~ 13 – A - close-up of the map of Ochoa et al. (2015) shown in Fig. 12~~5~~B modified in the Elche sub-basin area, based on our interpretation of the seismic profile SIMBAD 26 (S.26); the trace of this seismic profile is taken from Driussi et al., 2015. This sub-basin is subdivided by a NE-SW oriented structural high (the Elche high) in two sectors with the PLG evaporites to the NW and a MSC unit floored by the MES to the SE (possibly corresponding to MSC stage 2 RLG unit and overlying stage 3 deposits); the green dotted line represents the inferred PLG southern basin

950 margin, while the black dotted line interpreted by Ochoa et al. (2015) as the Messinian shelf
951 break represents its northern margin; B – interpretation of the SIMBAD 26 seismic profile shown
952 in Driussi et al. (2015); note the Messinian unit in the southeastward end of the profile; C – line
953 drawing of the SIMBAD 26 profile: the PLG unit (in violet) shows a lower concordant base; it is
954 and a truncated top. It correlates with the seismic unit (in violet) cut on top by the Messinian
955 erosional surface (MES) and occurring upslope of the area deformed and eroded possibly
956 corresponding to a Messinianthe Elche structural/volcanic high; beyond this structure, the
957 Messinian unit (in cyan) shows a basal unconformity (MES or MES-CC) and onlap terminations
958 against the eroded area; note the rapid thinning of layered deposits and the probable transition
959 to slope deposits. The two Messinian units were likely deposited in different times in areas
960 separated by a structural/volcanic feature pre-existing and/or uplifted during and still active
961 after the MSC; C - Schematic stratigraphic relationships between the MSC units recognized in the
962 Balearic Promontory (modified from Maillard et al., 2014). C1 – observed units and surfaces; C2-
963 C4 - new interpretation model with the MES developing on top of the BU-PLG unit and passing
964 downslope to the BES at the base of the Slope and BU units; C3 – detail of the possible facies
965 relationships between the stratified deposits of the BU (likely turbiditic) and the chaotic deposits
966 of the Slope Unit; note that the overall onlap of the BU deposits on the Slope unit is not
967 necessarily related to a different age of the two units and that the top of the latter is an irregular
968 surface, which does not necessarily correspond to a subaerial unconformity. CMD = Central
969 Mallorca Depression.C.
970
971 Fig. S1 – Table with the $^{87}Sr/^{86}Sr$ values obtained from selenite gypsum samples analysed in this
972 work: all the values fall in the range of the first stage of the salinity crisis. (A) simplified
973 geological map of the Garrucha-Coscojar area of the Sorbas-Vera basin (see Fig. 7b) with the

~~location of the samples; (B) simplified geological map of the Bajo Segura basin with the location of the main outcrop sections and boreholes crossing the PLG deposits; (C) Sedimentary logs of the Benejuzar and San Miguel de Salinas sections showing the location of samples for Sr isotope analysis; (D) Strontium isotope values framed in the Messinian Sr isotope stratigraphy; (E) stratigraphic framework of the MSC (modified from Manzi et al., 2013 and Roveri et al., 2014a).~~

~~Fig. 18~~ S214 ~~– Schematic stratigraphic relationships between the MSC units recognized in the Balearic Promontory (modified from Maillard et al., 2014). A – observed units and surfaces; B - new interpretation model with the MES developing on top of the BU-PLG unit and passing downslope to the BES at the base of the Slope and BU units; C – detail of the possible facies relationships between the stratified deposits of the BU (likely turbiditic) and the chaotic deposits of the Slope Unit; note that the overall onlap of the BU deposits on the Slope unit is not necessarily related to a different age of the two units and that the top of the latter is an irregular surface, which does not necessarily correspond to a subaerial unconformity. CMD = Central Mallorca Depression.~~

~~Table 1 – List of acronyms used in this work~~

Table 1 - List of acronyms used for the surfaces and the units of the Messinian salinity crisis (MSC) that can be identified in seismic (S), geophysical log (L), continuous cores (C) and outcrop (O).

Table 2 – Seismic parameters used for the synthetic seismic sections of the Sorbas (Fig. 9), Nijar (Fig. 10) and Belice (Fig. 11) basins.

Table ~~1~~ 32 – Synthesis of the main features (facies, depositional setting, geochemistry, thickness) of the Messinian units and surfaces and their expected seismic and borehole expression; the more common features are in bold; nd = not defined.

Table ~~2~~ 43 – Possible relationships of seismic facies to onshore Messinian units; note that there is no univocal relationship, in particular for the bedded facies.

Table ~~3~~ 54 - Characteristics and possible relationships with onshore equivalents of Messinian surfaces.

References

ARENAS, C. & POMAR, L. (2010) Microbial deposits in upper Miocene carbonates, Mallorca, Spain. *Palaeogeography, Palaeoclimatology, Palaeoecology* 297, 465–485.

BASSETTI, M.A., MICULAN, P. & SIERRO, F.S. (2006) Evolution of depositional environments after the end of Messinian salinity crisis in Nijar Basin (SE Betic Cordillera). *Sedimentary Geology* 188–189, 279–295.

BARRAGAN. G. (1986) Una nueva interpretación de la sedimentación neógena en el sector suroccidental de la Cuenca de Vera. *Acta Geologica Hispanica*, 21-22, 449-457.

BOURILLOT, R., VENNIN, E., ROUCHY, J.M., DURLET, C., ROMMEVAUX, V., KOLODKA, C. & KNAP, F. (2010) Structure and evolution of a Messinian mixed carbonate-siliciclastic platform: the role of evaporites (Sorbas Basin, South-east Spain*). Sedimentology* 57, 477–512.

BRAGA, J.C., MARTÍN, J.M. & WOOD, J.L. (2001) Submarine lobes and feeder channels of redeposited, temperate carbonate and mixed sliciclastic-carbonate platform deposits (Vera Basin, Almeria, southern Spain). *Sedimentology*, 48, 99-116.

BRAGA, J.C., MARTÍN, J.M., RIDING, R., AGUIRRE, J., SANCHEZ-ALMAZO, I.M. & DINARES-TURELL, J. (2006) Testing models for the Messinian salinity crisis: the Messinian record in Almería, SE Spain. *Sedimentary Geology*, 188–189, 131–154.

CIESM (2008) The Messinian salinity crisis from mega-deposits to microbiology. In: Briand, F. (Ed.), *A consensus report*, in 33ème CIESM Workshop Monographs, 33. CIESM, 16, bd de Suisse, MC-98000, Monaco, pp. 1–168.

CLAUZON, G., SUC, J.-P., GAUTIER, F., BERGER, A. & LOUTRE, M.-F. (1996) Alternate interpretation of the Messinian salinity crisis: controversy resolved? *Geology*, 24, 363–366.

CONESA, G., MARTIN, J.P.S., CORNÉE, J.J. & MULLER, J.P. (1999) Nouvelles contraintes sur la crise de salinite messinienne par l'etude d'une plate-forme carbonateée´e marginale (bassin de Sorbas, Espagne). *Compte Rendu Academie Science Paris*, 328, 81–87.

CORBI, H., SORIA, J.M., LANCIS, C., GIANNETTI, A., TENT-MANCLUS, J.E. & DINARES-TURELL, J. (2016) Sedimentological and paleoenvironmental scenario before, during, and after the Messinian Salinity Crisis: The San Miguel de Salinas composite section (western Mediterranean). *Marine Geology*, 379, 246-266.

CORNÉE, J.-J., SAINT MARTIN, J.-P., CONESA, G., MUNCH, P.H., ANDRÉ, J.-P., SAINT MARTIN, S. & ROGER, S. (2004) Correlation and sequence stratigraphic model for Messinian carbonate platforms of the western and central Mediterranean. *International Journal of Earth Sciences*, 93, 621-633.

DELA PIERRE, F., BERNARDI, E., CAVAGNA, S., CLARI, P., GENNARI, R., IRACE, A., LOZAR, F.,

LUGLI, S., MANZI, V., NATALICCHIO, M., ROVERI, M. & VIOLANTI, D. (2011) The record of the Messinian salinity crisis in the Tertiary Piedmont Basin (NW Italy): the Alba section revisited. *Palaeogeography, Palaeoclimatology, Palaeoecology*, 310, 238–255.

DI BLASI, F. (2018) Morphology and morphogenesis of modern subaqueous drainage systems: implications for the origin of the Mediterranean Messinian canyons. PhD Thesis, University of Parma, 261 pp.

DRIUSSI, O., MAILLARD, A., OCHOA, D., LOFI, J., CHANIER, F., GAULLIER, V., BRIAIS, A., SAGE, F., SIERRO, F. & GARCIA, M. (2015) Messinian Salinity Crisis deposits widespread over the Balearic Promontory: insights from new high-resolution seismic data. *Marine Petroleum Geology*, 66, 41-54.

DRONKERT, H. (1976) Late Miocene evaporites in the Sorbas basin and adjoining areas. *Memorie della Società Geologica Italiana*, 16, 203–243.

ETHEVE, N., FRIZON DE LAMOTTE, D., MOHN, G., MARTOS, R., ROCA, E. & BLANPIED (2016) Extensional vs contractional Cenozoic deformation in Ibiza (Balearic Promontory, Spain): Integration in the West Mediterranean back-arc setting. *Tectonophysics*, 682, 35-55.

FAGIN, S.W. (1991) Seismic Modeling of Geologic Structures: Applications to Exploration Problems. Society of Exploration Geophysicists, Tulsa, Oklahoma. Geophysical Development Series 2.

FORTUIN, A.R. & KRIJGSMAN, W. (2003) The Messinian of the Nijar basin (SE Spain): sedimentation, depositional environments and paleogeographic evolution. *Sedimentary Geology*, 160, 213–242.

FORTUIN, A.R., KELLING, J.M.D. & ROEP, T.B. (1995) The enigmatic Messinian–Pliocene section of Cuevas del Almanzora (Vera basin, SE Spain) revisited — erosional feature and strontium isotope ages. *Sedimentary Geology*, 97, 177–201.

GENNARI, R., IACCARINO, S.M., DI STEFANO, A., STURIALE, G., CIPOLLARI, P., MANZI, V., ROVERI, M. & COSENTINO, D. (2008) The Messinian–Zanclean boundary in the Northern Apennine. *Stratigraphy* 5, 307–322.

GENNARI, R., LOZAR, F., TURCO, E., DELA PIERRE, F., LUGLI, S., MANZI, V., NATALICCHIO, M., ROVERI, M., SCHREIBER, B.C. & TAVIANI, M. (2018) Integrated stratigraphy and paleoceanographic evolution of the pre-evaporitic phase of the Messinian salinity crisis in the Eastern Mediterranean as recorded in the Tokhni section (Cyprus Island). *Newsletter on Stratigraphy*, 51, 33-55.

GENNARI, R., MANZI, V., ANGELETTI, L., BERTINI, A., BIFFI, U., CEREGATO, A., FARANDA, C., GLIOZZI, E., LUGLI, S., MENICHETTI, E., ROSSO, A., ROVERI, M. & TAVIANI, M. (2013) A shallow water record of the onset of the Messinian salinity crisis in the Adriatic foredeep (Legnagnone section, Northern Apennines). *Palaeogeography, Palaeoclimatology, Palaeoecology*, 386, 145–164.

GOMEZ DE LA PEÑA, L., GRACIA, E., MUÑOZ, A., ACOSTA, J., GOMEZ-BALLESTEROS, M., RANERO, C.R. & UCHUPI, E. (2016) Geomorphology and Neogene tectonic evolution of the Palomares continental margin (Western Mediterranean). *Tectonophysics*, 689, 25-39.

GVIRTZMAN, Z., MANZI, V., CALVO, R., GAVRIELI, I., GENNARI, R., LUGLI, S., REGHIZZI, M. & ROVERI, M. (2017) Intra-Messinian truncation surface in the Levant Basin explained by subaqueous dissolution. *Geology*, 45, 915-918.

HILGEN, F.J., KUIPER, K.F., KRIJGSMAN, W., SNEL, E. & VAN DER LAAN, E. (2007) Astronomical tuning as the basis for high resolution chronostratigraphy: the intricate history of the Messinian Salinity Crisis, *Stratigraphy*, 4, 231-238.

HSÜ, K., RYAN, W.B.F. & CITA, M.B. (1973) Late Miocene desiccation of the Mediterranean.

Nature, 242, 240.

KASTENS, K.A., MASCLE, J. & AUROUX, C., et al. (1987) *Proceedings ODP*, Initial Reports, 107. College Station, TX (Ocean Drilling Program).

KRIJGSMAN, W., CAPELLA, W., SIMON, D., HILGEN, F.J., KOUWENHOVEN, T.J., MEJIER, P.Th., SIERRO, F.J., TULBURE, M.A., van den BERG, B.C.J., van der SCHEE, M. & FLECKER, R. (2018) The Gibraltar Corridor: Watergate of the Messinian Salinity Crisis. *Marine Geology*, 400, 238-246.

KRIJGSMAN, W., FORTUIN, A.R., HILGEN, F.J. & SIERRO, F.J. (2001) Astrochronology for the Messinian Sorbas Basin (SE Spain) and orbital (precessional) forcing evaporite cyclicity. *Sedimentary Geology*, 140, 43-60.

KRIJGSMAN, W., HILGEN, F., RAFFI, I., SIERRO, F., WILSON, D., 1999. Chronology, causes and progression of the Messinian salinity crisis. *Nature*, 400, 652–655.

LOFI, J., DÉVERCHÉRE, J., GAULLIER, V., GILLET, H., GORINI, C., GUENNOC, P., LONCKE, L., MAILLARD, A., SAGE, F. & THINON, I. (2011a) Seismic Atlas of the Messinian Salinity Crisis Markers in the Offshore Mediterranean Domain. *Commission for the Geological Map of the World and Memoires de la Société Géologique de France*, Nouvelle Série, p. 72.

LOFI, J., GORINI, C., BERNE, S., CLAUZON, G., DOS REIS, A.T., RYAN, W.B.F. & STECKLER, M.S. (2005) Erosional processes and paleo-environmental changes in the western Gulf of Lions (SW France) during the Messinian Salinity Crisis. *Marine Geology*, 217, 1–30.

LOFI, J., SAGE, F., DÉVERCHÈRE, J., LONCKE, L., MAILLARD, A., GAULLIER, V., THINON, I., GILLET, H., GUENNOC & P., GORINI, C. (2011b) Refining our knowledge of the Messinian salinity crisis records in the offshore domain through through multi-site seismic analysis. *Bulletin Societé Géologique de France* 182, 163–180.

LUGLI, S., GENNARI, R., GVIRTZMAN, Z., MANZI, V., ROVERI, M. & SCHREIBER, B.C. (2013) Evidence of clastic evaporites in the canyons of the Levant Basin (Israel): implications for the Messinian Salinity Crisis. *Journal of Sedimentary Research,* 83, 942–954.

LUGLI, S., MANZI, V., ROVERI, M. & SCHREIBER, C. (2010) The Primary Lower Gypsum in the Mediterranean: a new facies interpretation for the first stage of the Messinian salinity crisis. *Palaeogeography, Palaeoclimatology, Palaeoecology*, 297, 83–99.

LUGLI, S., MANZI, V., ROVERI, M. & SCHREIBER, C. (2015) The deep record of the Messinian salinity crisis: Evidence of a non-desiccated Mediterranean Sea. *Palaeogeography, Palaeoclimatology, Palaeoecology*, 433, 201–218.

MAILLARD, A., DRIUSSI, O., LOFI, J., BRIAIS, A., CHANIER, F., HÜBSCHER, C. & GAULLIER, V. (2014) Record of the Messinian Salinity Crisis in the SW Mallorca area (Balearic Promontory, Spain). *Marine Geology*, 357, 304–320.

MANZI V., GENNARI, R., LUGLI, S., PERSICO, D., REGHIZZI, M., ROVERI, M., SCHREIBER, B.C., CALVO, R., GAVRIELI, I. & GVIRTZMAN, Z. (2018) The onset of the Messinian salinity crisis in the deep Eastern Mediterranean Basin. *Terra Nova*, https://doi.org/10.1111/ter.1232530, 189-198.

MANZI V., LUGLI S., ROVERI M., DELA PIERRE F., GENNARI R. LOZAR F., NATALICCHIO M., SCHREIBER B.C., TAVIANI M. & TURCO E. (2016a) The Messinian salinity crisis in Cyprus: a further step towards a new stratigraphic framework for Eastern Mediterranean. *Basin Research* 28, 207-236.

MANZI, V., GENNARI, R., HILGEN, F., KRIJGSMAN, W., LUGLI, S., ROVERI, M. &, SIERRO, F.J., (2013).

Age refinement of the Messinian salinity crisis onset in the Mediterranean. *Terra Nova 25*, 315–322.

MANZI, V., LUGLI, S., RICCI LUCCHI, F. & ROVERI, M. (2005) Deep-water clastic evaporites deposition in the Messinian Adriatic foredeep (northern Apennines, Italy): did theMediterranean ever dry out? *Sedimentology* 52, 875–902.

MANZI, V., LUGLI, S., ROVERI, M. & SCHREIBER, B.C. (2009) A new facies model for the Upper Gypsum of Sicily (Italy): chronological and palaeoenvironmental constraints for the Messinian salinity crisis in the Mediterranean. *Sedimentology*, 56, 1937-1960.

MANZI, V., LUGLI, S., ROVERI, M., SCHREIBER, B.C. & GENNARI, R. (2011) The Messinian "Calcare di Base" (Sicily, Italy) revisited. *Geological Society of America Bulletin* 123, 347–370.

MANZI, V., ROVERI, M., GENNARI, R., BERTINI, A., BIFFI, U., GIUNTA, S., IACCARINO, S.M., LANCI, L., LUGLI, S., NEGRI, A., RIVA, A., ROSSI, M.E. & TAVIANI, M. (2007) The deep-water counterpart of the Messinian Lower Evaporites in the Apennine foredeep: the Fanantello section (Northern Apennines, Italy). *Palaeogeography, Palaeoclimatology, Palaeoecology*, 251, 470–499

MARTÍN, J.M. & BRAGA, J.C. (1994) Messinian events in the Sorbas basin in southeastern Spain and their implications in the recent history of the Mediterranean. *Sedimentary Geolog*y, 90, 257–268.

MARTÍNEZ DEL OLMO, W. (2011a) El arrecife Messiniense del sondeo Torrevieja Marino C.1 desde las linea sismicas (SE de Espana). *Revista Sociedad Geologica de Espana* 24, 173–185.

MARTÍNEZ DEL OLMO, W. (2011b) El Messiniense en el Golfo de Valencia y el Mar de Alborán: implicaciones paleogeográficas y paleoceanográficas. *Revista Sociedad Geologica de Espana*

24, 237–257.

MAS, G. (2015) El registre estratigrafic del Messinià terminal i del Pliocè a l'illa de Mallorca. Relacions amb la crisi de salinitat de la Mediterrània. Tesi Doctoral, Universitat de les Illes Balears, 1-534.

MAS, G.Y. & FORNÓS, J.J. (2012) La Crisis de Salinidad del Messiniense en la cuenca sedimentaria de Palma (Mallorca, Islas Baleares); The Messinian Salinity Crisis Record in the Palma basin (Mallorca, Balearic Islands*). Geogaceta* 52, 57–60.

MEILIJSON, A., STEINBERG, J., HILGEN, F., BIALIK, O.M., WALDMANN, N.D. & MAKOVSKY, Y. (2018) Deep-basin evidence resolves a 50-year-old debate and demonstrates synchronous onset of Messinian evaporites in a non-desiccated Mediterranean. *Geology* 46, 243-246.

MONTENAT, C. (1990) Les Bassins Neogenes du domain Betique oriental (Espagne). Tectonique et sedimentation dans un couloir de decrochement. Premier partie: etude regionale. *Doc. et Trav. IGAL, 12-13. IGAL*, Paris, 391 pp. + 3 maps.

OCHOA D., SIERRO F.J., LOFI J., MAILLARD A., FLORES J.-A. & SUAREZ M. (2015) Synchronous onset of the Messinian evaporite precipitation: First Mediterranean offshore evidence. *Earth and Planetary Science Letters* 427, 112-124.

OMODEO-SALÉ, S., GENNARI, R., LUGLI, S., MANZI, V. & ROVERI, M. (2012) Tectonic and climatic control on the Late Messinian sedimentary evolution of the Nijar Basin (Betic Cordillera, Southern Spain). *Basin Research* 24, 314–337.

ORSZAG-SPERBER, F. (2006) Changing perspectives in the concept of "Lago-Mare" in Mediterranean Late Miocene evolution. *Sedimentary Geology*, 188–189, 259–277.

REGHIZZI, M., GENNARI, R., DOUVILLE, E., LUGLI, S., MANZI, V., MONTAGNA, P, ROVERI, M., SIERRO, F. J., & TAVIANI, M. (2017) Isotope stratigraphy (87Sr/86Sr, δ18O, δ13C) of the

Sorbas basin (Betic Cordillera, Spain): paleoceanographic evolution across the onset of the Messinian salinity crisis. *Palaeogeography, Palaeoclimatology, Palaeoecology* 469, 60-73.

RIDING, R., BRAGA, J.C., MARTIN, J.M. & SANCHEZ-ALMAZO (1998) The Mediterranean Messinian Salinity Crisis: constraints from a coeval marginal basin, Sorbas, southeastern Spain. *Marine Geology* 146, 1-20.

ROEP, Th.B., DABRIO, C.J., FORTUIN, A.R. & POLO, M.D. (1998). Late highstand patterns of shifting and stepping coastal barriers and washover fans (late Messinian, Sorbas Basin, SE Spain). *Sedimentary Geology* 116, 27-56.

ROSELL, L., ORTÌ, F., KASPRZYK, A., PLAYA, E. & PERYT, T.M. (1998) Strontium geochemistry of Miocene primary gypsum: Messinian of Southeastern Spain and Sicily and Badenian of Poland. *Journal of Sedimentary Research* 68, 63-79.

ROUCHY, J.M. & CARUSO, A. (2006) The Messinian salinity crisis in the Mediterranean basin: a reassessment of the data and an integrated scenario. *Sedimentary Geology* 188-189, 33-67.

ROVERI M., LUGLI S, MANZI V, GENNARI R., IACCARINO S.M, GROSSI F. & TAVIANI M. (2006a) The record of Messinian events in the Northern Apennines foredeep basins. *Acta Naturalia de L'ateneo Parmense* 42, 47-123.

ROVERI M., MANZI V., LUGLI S., SCHREIBER B.C., CARUSO A., ROUCHY J.M., IACCARINO S.M., GENNARI R., VITALE F.P. & RICCI LUCCHI F. (2006b) Clastic vs. primary precipitated evaporites in the Messinian Sicilian basins. *Acta Naturalia de L'ateneo Parmense* 42, 125-199.

ROVERI, M., BASSETTI, M.A. & RICCI LUCCHI, F. (2001) The Mediterranean Messinian Salinity Crisis: an Apennine foredeep perspective. *Sedimentary Geology* 140, 201–214.

ROVERI, M., BERTINI, A., COSENTINO, D., DI STEFANO, A., GENNARI, R., GLIOZZI, E., GROSSI, F., IACCARINO, S.M., LUGLI, S., MANZI, V. & TAVIANI, M. (2008a) A high-resolution stratigraphic framework for the latest Messinian events in the Mediterranean area. *Stratigraphy* 5, 323–342.

ROVERI, M., BOSCOLO GALLO, A., ROSSI, M., GENNARI, R., IACCARINO, S.M., LUGLI, S., MANZI, V., NEGRI, A., RIZZINI, F. & TAVIANI, M. (2005) The Adriatic foreland record of Messinian events (Central Adriatic Sea, Italy). *GeoActa* 4, 139-158.

ROVERI, M., FLECKER, R., KRIJGSMAN, W., LOFI, J., LUGLI, S., MANZI, V., SIERRO, F.J., BERTINI, A., CAMERLENGHI, A. & DE LANGE, G. (2014a) The Messinian Salinity Crisis: past and future of a great challenge for marine sciences. *Marine Geology* 352, 25–58.

ROVERI, M., GENNARI, R., LUGLI, S. & MANZI, V. (2009) The Terminal Carbonate Complex: the record of sea-level changes during the Messinian salinity crisis. *GeoActa* 8, 57–71.

ROVERI, M., GENNARI, R., LUGLI, S., MANZI, V., MINELLI, N., REGHIZZI, M., RIVA, A., ROSSI, M.E. & SCHREIBER, B.C. (2016) The Messinian salinity crisis: open problems and possible implications for Mediterranean petroleum systems. *Petroleum Geoscience* 22, 283-290.

ROVERI, M., GENNARI, R., PERSICO, D., ROSSI, F.P., LUGLI, S., MANZI, V., REGHIZZI, M. & TAVIANI, M. (2018) A new chronostratigraphic and palaeoenvironmental framework for the end of the Messinian salinity crisis in the Sorbas Basin (Betic Cordillera, southern Spain). *Geological Journal* DOI: 10.1002/gj.3256.

ROVERI, M., LUGLI, S., MANZI, V. & SCHREIBER, B.C. (2008b) The Messinian Sicilian stratigraphy revisited: toward a new scenario for the Messinian salinity crisis. *Terra Nova* 20, 483–488.

ROVERI, M., LUGLI, S., MANZI, V. & SCHREIBER, B.C. (2008c) The shallow- to deep-water record of the Messinian salinity crisis: new insights from Sicily, Calabria and Apennine basins. In: CIESM 2008. *The Messinian Salinity Crisis from Mega-deposits to Microbiology – A Consensus Report* (Ed. F. Briand), CIESM Workshop Monographs, 33, 72–82. Monaco.

ROVERI, M., LUGLI, S., MANZI, V., GENNARI, R. & SCHREIBER, B.C. (2014b) High-resolution strontium isotope stratigraphy of the Messinian deep Mediterranean basins: implications for marginal to central basins correlation. *Marine Geology* 349, 113–125.

ROVERI, M., MANZI, V., BERGAMASCO, A., FALCIERI, F., GENNARI, R. & LUGLI, S. (2014c) Dense shelf water cascading and Messinian canyons: a new scenario for the Mediterranean salinity crisis. *American Journal of Science* 314, 751-784.

ROVERI, M., MANZI, V., RICCI LUCCHI, F. & ROGLEDI, S. (2003) Sedimentary and tectonic evolution of the Vena del Gesso Basin (Northern Apennines, Italy): implications for the onset of the Messinian salinity crisis. *Geological Society of America Bulletin* 115, 387–405.

RYAN, W.B.F. & CITA, M.B. (1978) The nature and distribution of Messinian erosion surfaces, indicators of a several-kilometer-deep Mediterranean in the Miocene. *Marine Geology* 27, 193-230.

SANZ DE GALDEANO, C. (1990) Geologic evolution of the Betic Cordilleras in the Western Mediterranean, Miocene to the present. *Tectonophysics* 172, 107–119.

SIERRO, F., HILGEN, F., KRIJGSMAN, W. & FLORES, J. (2001) The Abad composite (SE Spain): a Messinian reference section for the Mediterranean and the APTS. *Palaeogeography, Palaeoclimatology, Palaeoecology* 168, 141–169.

SORIA, J.M., CARACUEL, J.E., CORBÌ, H., DINARÈS-TURELL, J., LANCIS, C., TENT-MANCLÙS, J. & YÉBENES, A. (2008) The Bajo Segura Basin (SE Spain): implications for the Messinian Salinity Crisis in the Mediterranean margins. *Stratigraphy* 5, 259–265.

STOICA, M., KRIJGSMAN, W., FORTUIN, A. & GLIOZZI, E. (2016) Paratethyan ostracods in the Spanish Lago-Mare: more evidence for interbasinal exchange at high Mediterranean sea level. *Palaeogeography, Palaeoclimatology, Palaeoecology* 441, 854-870.

VAI, G.B. (1997) Cyclostratigraphic estimate of the Messinian Stage duration. In: Montanari, A., Odin, G.S., Coccioni, R. (Eds.), *Miocene Stratigraphy: An Integrated Approach*. Developments in Paleontology and Stratigraphy 15, 463–476.

VAI, G.B. & RICCI LUCCHI, F. (1977) Algal crusts, autochtonous and clastic gypsum in a cannibalistic evaporite basin; a case history from the Messinian of Northern Apennine. *Sedimentology* 24, 211–244.

VOLK, H.R. (1967) Zur Geologie und Stratigraphy des Neogenbekkens von Vera, Südost Spanien. —Doctor's Thesis Univ. Amsterdam: 1-164.

acronym	S	L	C	O	corresponding names
BES	•				**Bottom Erosion Surface** (erosional base of MSC-related offshore seismic units)
BS	•				**Bottom Surface** (base of MSC-related offshore seismic units)
BU	•				**Bedded Unit** (generic MSC-related seismic unit characterized by parallel, continuous reflections)
EOS		•	•	•	**Evaporite Onset Surface** (local base of PLG)
FBI			•	•	**Foraminifera-barren interval** (lateral, deep-water equivalent of PLG evaporites)
IES	•				**Intermediate Erosion Surface** (erosional surface within MSC-related offshore seismic units)
LU	•				**Lower Unit** (the lowest MSC-related seismic unit recognized in offshore settings)
M/P			•	•	**Miocene/Pliocene** boundary
MES	•	•	•	•	**Messinian Erosional Surface** (the main Messinian erosional surface, both subaerial and subaqueous, developed along the Mediterranean margins after the stage 1 of the salinity crisis)
MES-cc			•	•	**Messinian Erosional Surface correlative conformity** (the conformable surface of basinal settings that can be traced upslope into the MES)
MU	•				**Mobile Unit** (transparent seismic unit interpreted as halite, usually found above the LU or at the base of the offshore MSC-related succession)
OS			•	•	**Onset Surf**ace (onset of the salinity crisis; may locally coincide with EOS)
PLG		•	•	•	**Primary Lower Gypsum** (primary in situ evaporites – selenite gypsum – accumulated during the stage 1 of the salinity crisis in shallow-water basins)
RLG		•	•	•	**Resedimented Lower Gypsum** (complex of clastic and/or in situ primary gypsum, halite, limestone breccia and siliciclastic deposits accumulated during the stage 2 of the salinity crisis in deep-water settings)
SU	•				**Slope Unit** (MSC-related offshore seismic unit with chaotic or parallel reflections along slopes)
TCC			•	•	**Terminal Carbonate Complex** (Messinian mixed siliciclastic-carbonate platforms)
TES	•				**Top Erosion Surface** (erosional top of MSC-related offshore seismic units)
TS	•				**Top Surface** (top of MSC-related offshore seismic units)
UG		•	•	•	**Upper Gypsum** (primary in situ evaporites – selenite gypsum – accumulated during stage 3 of the salinity crisis in shallow-water basins)
UU	•				**Upper Unit** (the uppermost MSC-related seismic unit in offshore settings)

lithology	p velocity m/sec	density g/cm^3	acoustic impedance	section	lithostratigraphic units
shales	1800	2.20	3960	Sorbas	Zorreras Mb., Chozas Fm., Sorbas Mb.
sandstones	2500	2.30	5750	Sorbas	Sorbas Mb.
	1900	2.00	3800	Belice	Belice Fm.
conglomerates	2500	2.10	5250	Sorbas	Gochar Fm., TCC2
	3250	2.10	6825	Nijar	Feos Fm.
	"	"	"	Belice	Terravecchia Fm.
clayey marls	2200	2.30	5060	Nijar	Feos Fm.
	2400	2.40	5760	Belice	Terravecchia Fm., Belice Fm.
marly sst	1750	2.00	3500	Sorbas	Chozas Fm.
	"	"	"	Nijar	Cuevas Fm.
calcareous sst	2700	2.30	6210	Sorbas	TCC1
marls	2500	2.35	5875	Sorbas	Fringing Reef, TCC1, Abad Mb, Yesares Mb.
	"	"	"	Nijar	Yesares Mb.
	"	"	"	Belice	Lagomare (Belice)
calcareous marls	3000	2.50	7500	Belice	Trubi Fm.
limestones	4200	2.40	5250	Sorbas	Bioherm Unit, Fringing Reef, Azagador Mb.,
	4750	2.55	12112.5	Nijar	Cantera Mb., Feos Fm.
	"	"	"	Belice	Terravecchia Fm.
anhydrites	4750	2.95	14012.5	Sorbas	Yesares Mb.
	"	"	"	Nijar	Feos Mb.
	"	"	"	Belice	PLG-RLG
chaotic deposits	3000	2.50	7500	Belice	RLG chaotic
schists	4800	2.85	13680	Sorbas	Basement
	"	"	"	Nijar	

MSC stage	unit - lithology	depositional setting, distribution	seismic facies		thickness twtt (sec) *m*	bounding surfaces		well logs		core/cuttings		
						bottom	top	RES/*GR*	pattern	$^{87}Sr/^{86}Sr$	sedimentology	fossils
1	**PLG** - primary gypsum (selenite)/mudstone layered evaporites	shallow silled basins **basinward of shoreline/shelf break**	high-amplitude parallel reflectors ***("bedded")***	apparent basal onlap and internal discordances apparent chaotic reflectors (CU) in the upper part	0-0.15 *0-300*	**concordant** **EOS** (diachronous)	**erosional angular discordance** concordant **MES**	high/*very low*	**blocky**	**>0.709088** (gypsum, carbonate)	very thick massive or **branching** selenite deposits	bacterial mats, mollusk
	FBI - Foraminifer-barren interval, dark organic-rich mudstones and dolostones (CdB-2)	deeper water silled basins, **open shelves and slopes, deep basin**	transparent to low amplitude reflectors ***("weakly bedded")***	**often below seismic resolution**	0-0.05 *0-50*	**concordant** **OS** (synchronous)	concordant, **erosional, angular discordance MES**	low/*high*	irregular or cyclic	**>0.709088** (carbonate)	organic-rich mudstones peloidal carbonates.	bacterial mats, c. nannoplancton, diatoms. **forams barren**
	carbonate ramps and reefs	coastal to shallow marine **landward of PLG**	high-amplitude **offlapping** reflectors	forestepping angular or tangential basal downlap	0-0.2 *0-200*	**downlap** ***nd***	**erosional** angular discordance **MES**	moderate/*low*	blocky to irregular	**≥0.709088** (carbonate)	grainstone, oolites	Porites, Halimeda
2	**RLG** – primary (cumulate) **- layered Halite, K-salt** – massive to thin layered	intermediate to deep basins **detached from PLG basins** chaotic deposits along basin margins and slopes	high to low-amplitude parallel reflectors ***("bedded")*** **transparent** (halite)	possible giant-size PLG olistoliths within CU; appearing as discontinuous BU units bounded by BES and TES blocky pattern in well logs	0-1.0 *0-2000*	concordant **MES-CC** **erosional angular discordance** **MES**	**concordant**	high/ *low (halite) or high (K-salts)*	**blocky**	**>0.709088** (Salt, gypsum, carbonate)	cm- to dm-thick bands, minor anhydrite	**mostly barren**
	RLG – primary (cumulate) and **clastic gypsum**/anhydrite		high to low-amplitude parallel reflectors ***("bedded")***		0-0.25 *0-500*			high/*very low*	**spiky**		mm-thick laminites graded beds	
	RLG – limestone breccia (CdB-3) – massive to layered		**lenticular**		0-0.05 *0-50*			moderate/*low*			clay chips, pellets	
	RLG - clastics (turbidites) - layered		high to low-amplitude parallel reflectors ***("bedded")***		0-0.25 *0-500*						graded beds	
	RLG -chaotic deposits (olistostromes, slides) - massive		**chaotic** to irregular and discontinuous reflectors **transparent** (shale)		0-0.5 *0-1000*		weakly erosional or irregular	irregular	irregular		selenite blocks (olistoliths), folds	
3	**UG – primary gypsum** (**selenite**)/mudstone, clastic, fluvio-deltaic - layered	shallow marginal basins usually **above RLG** and/or **onlapping eroded PLG** or older deposits	high to low-amplitude parallel reflectors ***("bedded")***	internal sharp or weakly erosional surfaces (in evaporite-free deposits) forestepping – stage 3.1 backstepping – stage 3.2	0-0.15 *0-300*	erosional - **MES** concordant on RLG - ***nd***	concordant **M/P**	high/*very low*	**spiky**	**<0.709088** (gypsum, limestone, shells)	gypsum selenite, cumulate	**Lagomare mollusks, ostracods, dinocysts**
	mudstones, turbiditic sandstones and/or cumulate/clastic gypsum - layered	intermediate to deep basins, **detached from PLG basins**	low-amplitude parallel reflectors ***("weakly bedded")*** transparent	**often below seismic resolution**	0-0.5 *0-1000*	erosional- **MES** concordant on RLG - ***nd***	concordant **M/P**	low/*high*	**spiky**		**gypsum-free** clastic or cumulite gypsum	

seismic facies	offshore unit	onshore unit	MSC stage
high-amplitude parallel reflectors *(“bedded”)*	**BU, UU**	PLG layered evaporites	**1**
	BU, LU, UU	RLG layered evaporites, layered siliciclastics	**2**
	BU, UU	UG layered evaporites, layered siliciclastics	**3**
transparent to low amplitude reflectors *(“weakly bedded”)*	**MU**	RLG massive to thin layered halite	**2**
		PLG layered evaporites (thickest cycles)	
chaotic, discontinuous high to low amplitude reflectors	**CU**	PLG – layered evaporites (upper cycles, low resolution seismic)	**1**
		RLG olistostromes, submarine slides, coarse-grained siliciclastics	**2**
		PLG-UG layered evaporites (low resolution seismic)	**3**
	SU	Carbonate ramp, reef slope, terrigenous slope, chaotic deposits	**1, 2, 3**

surface type	terminations		offshore surfaces (Lofi et al., 2011a,b)	onshore surfaces	stratigraphic position
	below	above			
major erosional/onlap (locally angular discordance)	truncation	onlap	**TES** *(top erosion surface)*	MES (top PLG)	top stage 1
				unnamed (top RLG chaotics)	top stage 2
			BES *(bottom erosion surface)*	MES (bottom RLG or clastics)	base stage 2
				MES (base UG or clastics)	base stage 3
	sharp	onlap (apparent)		EOS/OS (base PLG)	base stage 1
minor erosional/onlap	sharp/erosional	onlap, converging	**IES** *(intermediate erosion surface)*	pinch-out of thicker PLG cycles (3-5)	stage 1 PLG unit
	truncation	onlap		base of evaporite-bearing gravity flow (channelized or unchannelized)-RLG, UG	stage 2 RLG unit , stage 3 UG unit
	irregular	onlap	**TES** *(top erosion surface)*	RLG chaotic-UG/Lagomare transition	top stage 2
sharp, non-erosional surfaces	concordant	concordant	**BS** *(bottom surface)*	EOS/OS (PLG base)	base stage 1
				MES-CC (RLG base)	base stage 2
			TS *(top surface)*	unnamed, RLG-stage 3 transition	base stage 3
				M/P, stage 3-Pliocene transition	top stage 3

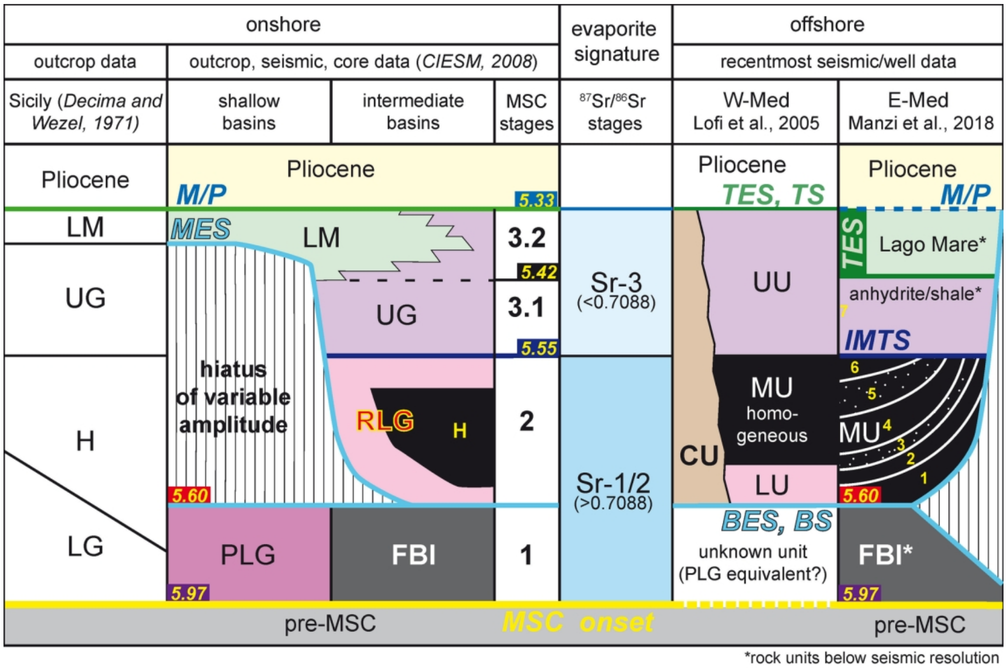

Fig. 1 – Tentative onshore-offshore correlation of the Messinian units and surfaces (modified from Roveri et al., 2014b).

152x101mm (300 x 300 DPI)

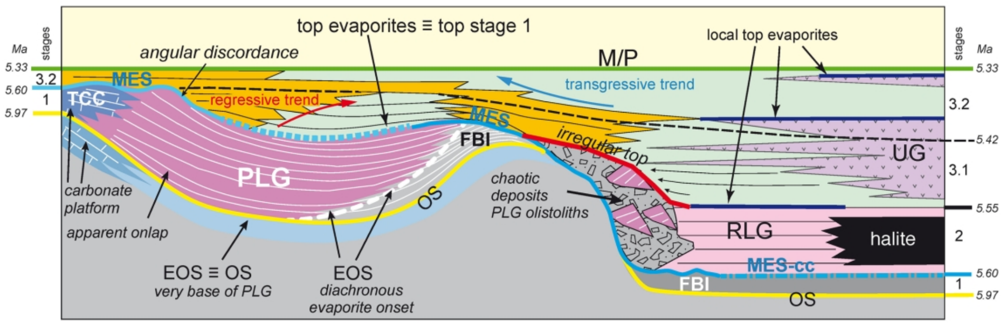

Fig. 2 – Conceptual stratigraphic model of the Messinian deposits of shallow and intermediate depth sub-basins. PLG = Primary Lower Gypsum; FBI = foraminifer-barren unit; RLG = Resedimented Lower Gypsum; UG = Upper Gypsum; MES = Messinian erosional surface; MES-cc = correlative conformity; M/P = Messinian-Pliocene boundary; OS = onset surface of the Messinian salinity crisis; EOS = evaporite onset surface; TCC = Terminal Carbonate Complex.

185x59mm (300 x 300 DPI)

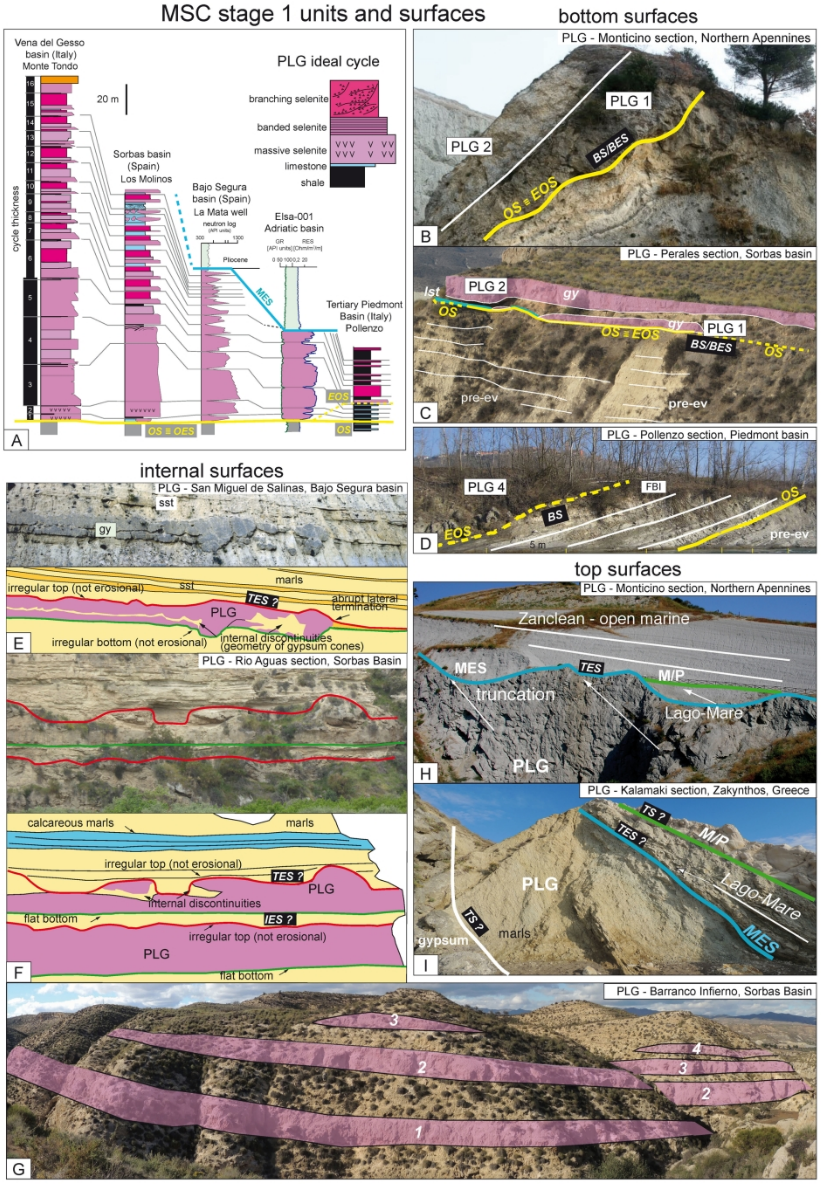

Fig. 3 – Stage 1 deposits and surfaces: outcrop examples. Black labels refer to the possible corresponding offshore markers (see chapter 3.4); A) the Primary Lower Gypsum (PLG) cycle model and the stacking pattern of PLG unit in outcrop and borehole sections; note the thinner basal cycles (1-2), the thicker cluster of cycles 3-4-5, the facies change at cycle 6 and the typical blocky pattern in well logs; Elsa 1 well shows a top-missing PLG record (due to erosion); in the Pollenzo section (see D) onset of evaporite deposition is delayed; in this case the onset of evaporites (EOS) is not coincident with the onset of the salinity crisis (OS). Bottom surfaces - B) Monticino section (Northern Apennines, Italy): base of PLG unit (BS) with the two lowermost thinner cycles; MSC onset and evaporite onset are coincident; C) Perales section (Sorbas basin, Southern Spain): laterally discontinuous gypsum lenses within PLG cycle 1, resulting in the local coincidence of OS and EOS surfaces (BS/BES); D) the Pollenzo section shown in A): white lines corresponds to the base of precessional cycles within the FBI unit and corresponding to PLG cycles 1 to 4; PLG onset (BS) occurred only at cycle 5. Internal surfaces - E) San Miguel de Salinas section (Bajo Segura basin, Spain) and F) Rio Aguas section (Sorbas Basin, Southern Spain): irregular top surface and abrupt lateral closures of gypsum beds due to the depositional geometry of growing selenite gypsum simulating erosional features (IES or

TES); note the contrast between the flat basal and the irregular top surfaces of individual gypsum beds; G) Barranco de Infierno (Sorbas Basin, Southern Spain): upper part of the Yesares Mb. showing the lenticular geometry of uppermost gypsum beds passing laterally to limestone and marls (IES or TES). Top surfaces - H) Monticino section (Northern Apennines, Italy) and I) Krystal Beach section (Zakynthos, Greece): the subaerial erosional surface (MES) developed on top of the tilted PLG unit sealed by uppermost stage 3 (Lago-Mare) and Zanclean open marine deposits.

181x258mm (300 x 300 DPI)

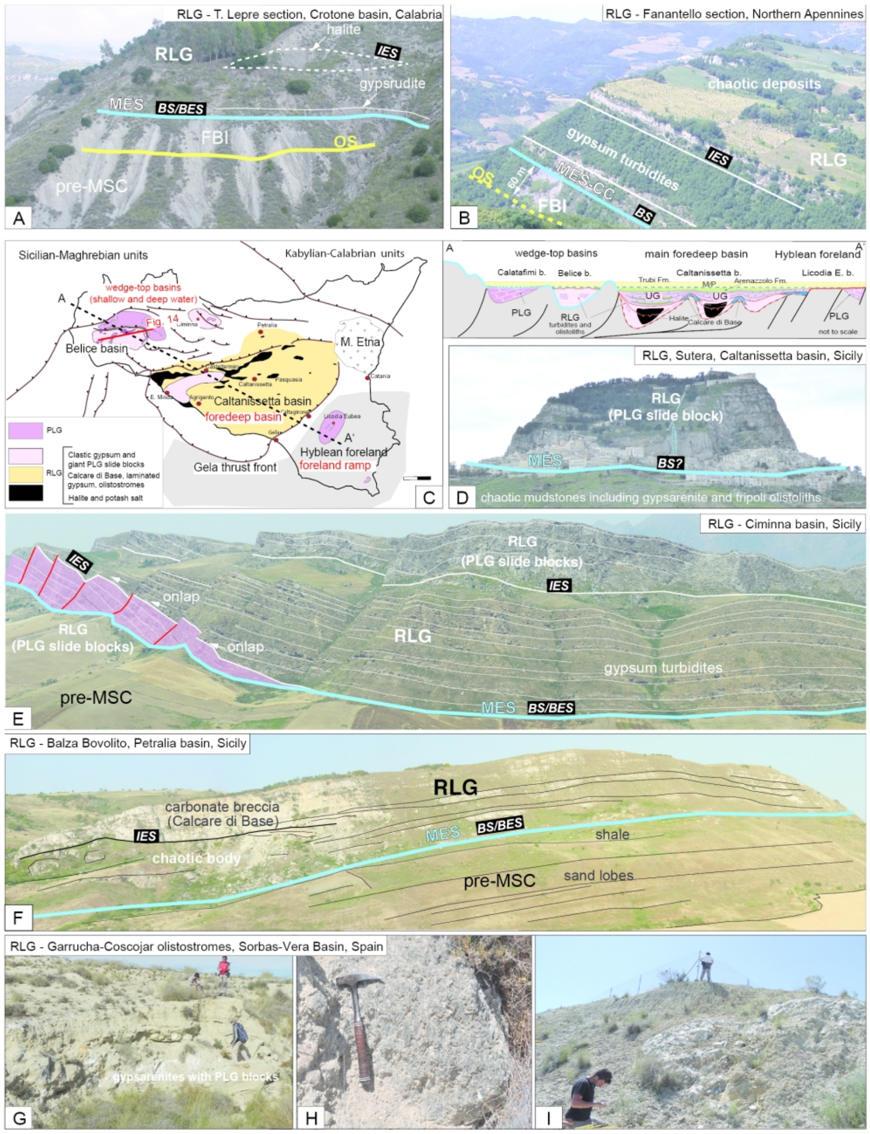

Fig. 4 – Stage 2 deposits and surfaces: outcrop examples. Black labels refer to the possible corresponding offshore markers (see chapter 3.4); A) T. Lepre section (Crotone basin, Calabria, Italy); here the MES partially erodes the MSC stage 1 FBI unit; the RLG unit consists of clastic gypsum enclosing small halite bodies; B) Fanantello section (Northern Apennines, Italy) showing the FBI sharply overlain by RLG deposits consisting of a basal stratified gypsarenite unit, in turn overlain by chaotic deposits with gypsum olistoliths; C) simplified geological map and cross-section of Sicily (from Roveri et al., 2008); D) Sutera (Caltanissetta basin, Sicily); the village lies at the base of a huge PLG block floating on a chaotic mudstone matrix including olistoliths of gypsarenites and diatomites, resting upon pre-MSC deposits; E) Ciminna basin (Sicily); horizontally stratified RLG gypsarenites and gypsrudites onlapping tilted PLG blocks and overlain by a second unit made of PLG slide blocks (from Roveri et al., 2008); F) Balza Bovolito (Petralia basin, Sicily); RLG stratified gypsarenites passing upward to stratified calcirudites and calcarenites; these deposits onlap and/or pass laterally to chaotic deposits and massive limestone breccia (modified from Manzi et al., 2011); G) Garrucha olistostrome (Sorbas-Vera basin, Spain; location in Fig. 7b,c)); gypsarenite and gypsrudite beds with gypsum olistoliths in the Garrucha olistostrome; H) PLG block, not in situ, included in the

Garrucha-Coscojar olistostrome; I) large recrystallized PLG block in the Coscojar olistostrome (Sorbas-Vera basin, Spain; location in Fig. 7b).

190x235mm (300 x 300 DPI)

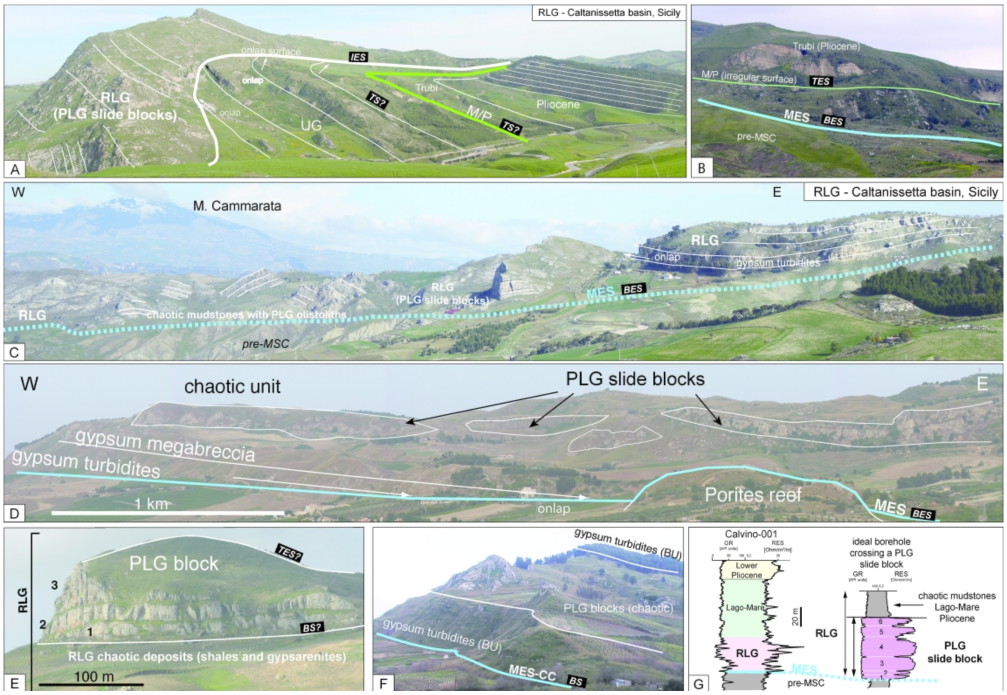

Fig. 5 – Stage 2 deposits and surfaces: outcrop examples. Black labels refer to the possible corresponding offshore markers (see chapter 3.4); A) Passo Fonnuto (Caltanissetta basin, Sicily); onlap of uppermost UG and Pliocene deposits against PLG slide blocks floating on top of a chaotic unit; ~1 km to the right a halite body is present under the river alluvional cover; B) Belice basin (Sicily); PLG blocks in a chaotic matrix directly overlain by lower Pliocene Trubi; C) nearby Racalmuto (Caltanissetta basin, Sicily); the RLG unit consists here of a basal chaotic body with large PLG blocks embedded in a mudstone matrix; stratified gypsarenites and gypsrudites onlap the PLG blocks; D) Santa Ninfa (Belice basin, Sicily); panoramic view showing the relationships between the stratified gypsum turbidites and the overlying chaotic deposits including large size PLG blocks and the pre-evaporitic unit; note the onlap of turbidites against a small lower Messinian Porites reef; E) Rocca delle Penne (Belice basin, Sicily); a giant PLG olistolith floating within a chaotic mass consisting of disarticulated and chaotic shales, gypsarenites, gypsrudites and marls; note the size of the olistolith which in this case includes the three basal cycles simulating a in situ PLG unit; the bottom and top surfaces of this body, if imaged in seismic profiles and/or crossed by boreholes, could be interpreted as BS/BES and TES, respectively ; F) Belice basin (Sicily), close to E), a chaotic unit with PLG blocks sandwiched by gypsum turbidites forming a tabular, stratified unit (compare with synthetic section of Fig. 14); G) the typical spiky well log facies of RLG deposits; the figure also shows the possible close association with a PLG block.

261x179mm (300 x 300 DPI)

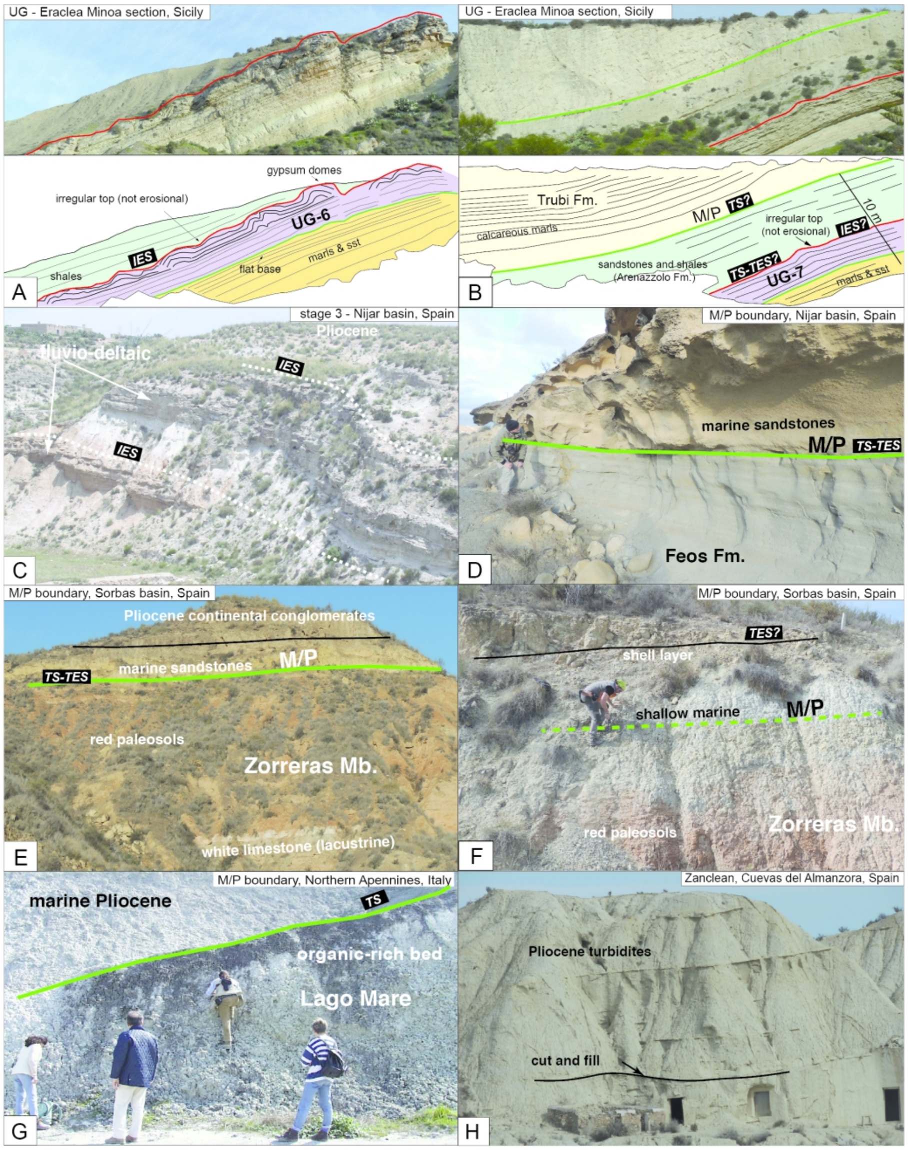

Fig. 6 – Stage 3 deposits and surfaces: outcrop examples. Black labels refer to the possible corresponding offshore markers (see chapter 3.4); A) Eraclea Minoa section (Sicily); irregular top of the 6th gypsum bed in the Upper Gypsum unit due to the domal growth geometry of gypsum crystals (IES/TES); B) location as A); the M/P boundary (corresponding to the Zanclean GSSP) occurs slightly above the irregular top of the topmost, 7th, UG bed; TS/TES is not coincident with the end of MSC; notice the presence of terrigenous fluvio-deltaic deposits in light green and orange in both the pictures; C) Nijar basin (Southern Spain); the cyclic stacking pattern of fluvio-deltaic and lacustrine deposits of MSC stage 3 Feos Fm.; strong reflectors are expected at the sharp transition from conglomerates to basinal marls; D) same location of C); transition to marine Pliocene deposits in the Los Castellones section; the Pliocene transgression in the Zorreras E) and la Cumbre F) sections (Sorbas basin); G) the organic-rich black layer marking the Miocene-Pliocene boundary in the Northern Apennines (Italy); H) Zanclean marls with thin-bedded turbidites in the Cuevas del Almanzora section (Vera basin); note the lenticular geometry of sandstone beds and the cut and fill structures, resulting in minor erosional surfaces.

174x230mm (300 x 300 DPI)

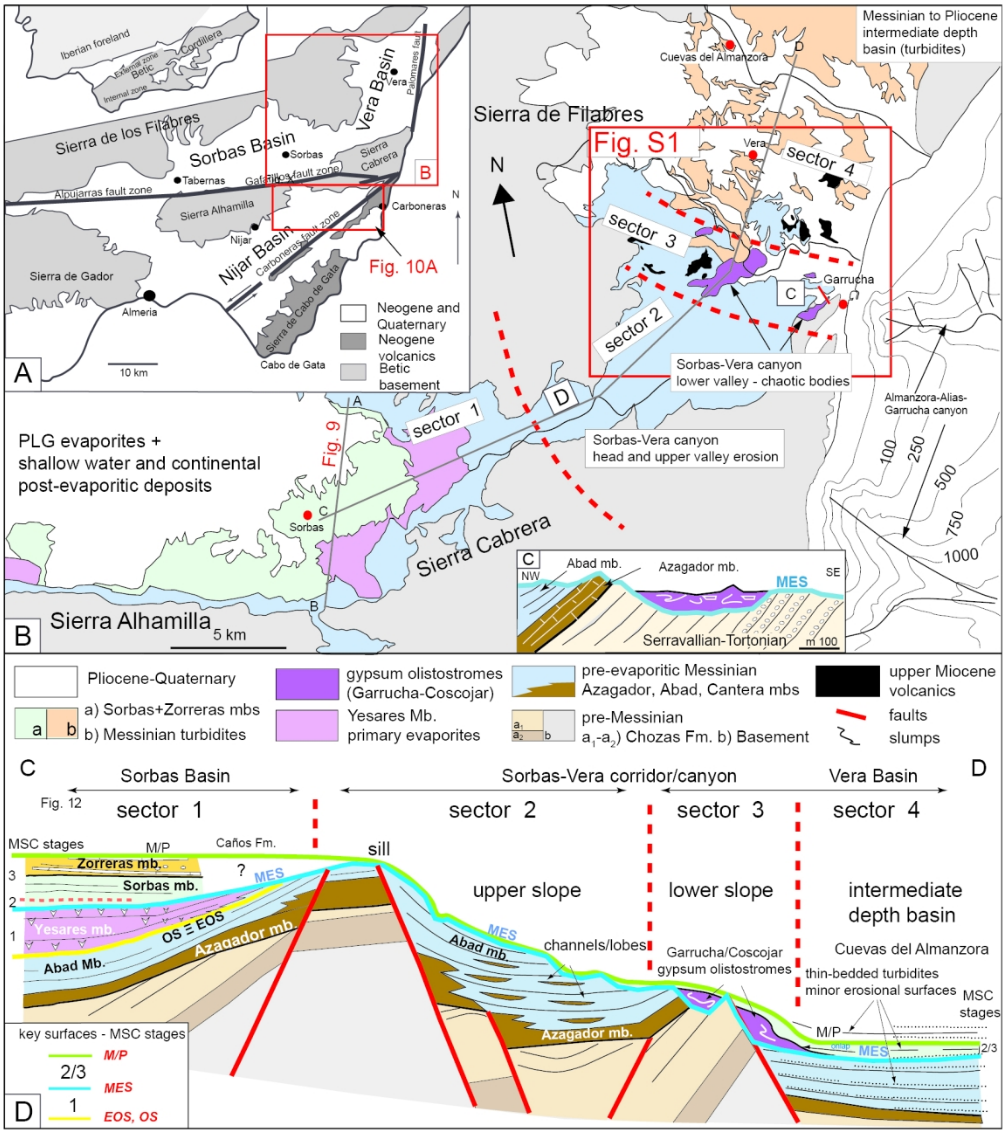

Fig. 7 – Schematic geological map of Southern Spain (A) with location of the Sorbas-Vera (B) and Nijar sub-basins (Fig. 10). (C) cross section showing that the Garrucha body was emplaced in an erosional depression cut in the underlying pre-MSC tilted succession (modified after Fortuin et al., 1995; Di Blasi, 2018); (D) Cross-section along the Sorbas-Vera basin. Notice the sill and the narrow, steep slope separating the shallow Sorbas sub-basin (Sector 1) and the deeper Vera sub-basin (Sector 4). The Sorbas-Vera corridor is here interpreted as a possible Messinian canyon showing an upper erosional tract (Sector 2) and a lower one with chaotic deposits (Sector 3; Garrucha olistostrome in the area shown in Fig. 8a,b); turbiditic lobes are developed in the slope base area and in the Vera sub-basin (Sector 4) .

152x171mm (300 x 300 DPI)

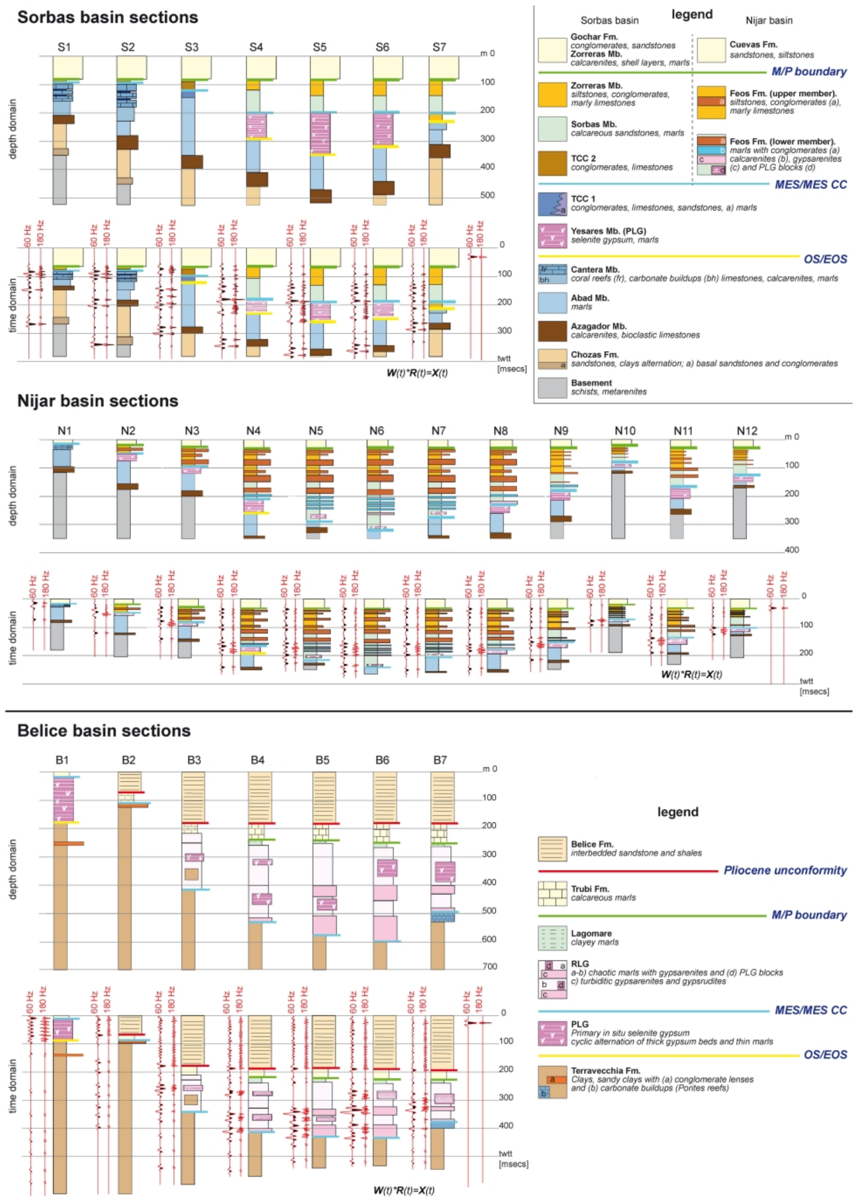

Fig. 8 – Stratigraphic logs and seismic wavelets used for the reconstruction of the synthetic seismic sections of the Sorbas (a), Nijar (b) and Belice (c) basins; the logs are shown in real depth and after transformation in time domain through the seismic parameters listed in Table 2. For each log in time domain, the resulting wavelets at 60 and 180 Hz are shown.

209x296mm (300 x 300 DPI)

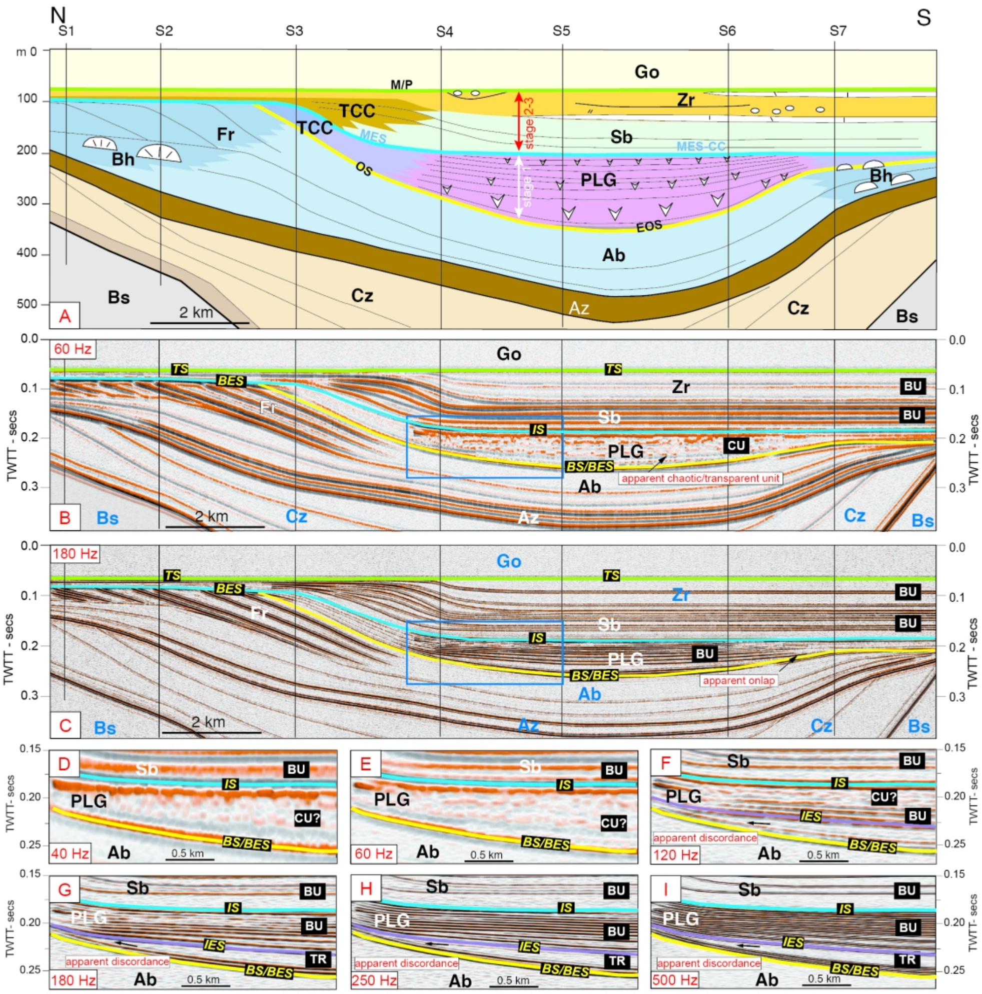

Fig. 9 – Sorbas basin synthetic seismic section (see also Fig. 8a); A) geological cross-section in depth domain (see location and legend in Fig. 7b; modified from Roveri et al., 2009) with the location of the hypothetical boreholes used for the reconstruction of synthetic seismic section; B-C) the synthetic seismic section in time domain with different dominant frequency: 60 Hz (B) and 180 Hz (C) resulting in different seismic resolution; black labels show the possible offshore units (white) and surfaces (yellow). In (D-I) a close-up of the PLG unit is shown with different seismic resolution; it is worth noting how the seismic aspect is function of the adopted frequency. At low frequencies of 40 and 60 Hz (D-E) the PLG appears as a chaotic/transparent unit. Starting from 120 Hz (F) PLG appears as a bedded unit (BU) only in its basal part; for a full resolution, higher frequencies between 180 (G) and 250 Hz (H) are needed; at 500 Hz (I) even the thinner beds are visible. In (F-I) a transparent unit in the lower part of the BU-PLG unit corresponds to the thickest PLG cycle 3; its lateral pinchout results in an apparent discordance; in this case both the PLG base and the top of cycle 3 could be erroneously interpreted as unconformities (BES and IES, respectively).

196x199mm (300 x 300 DPI)

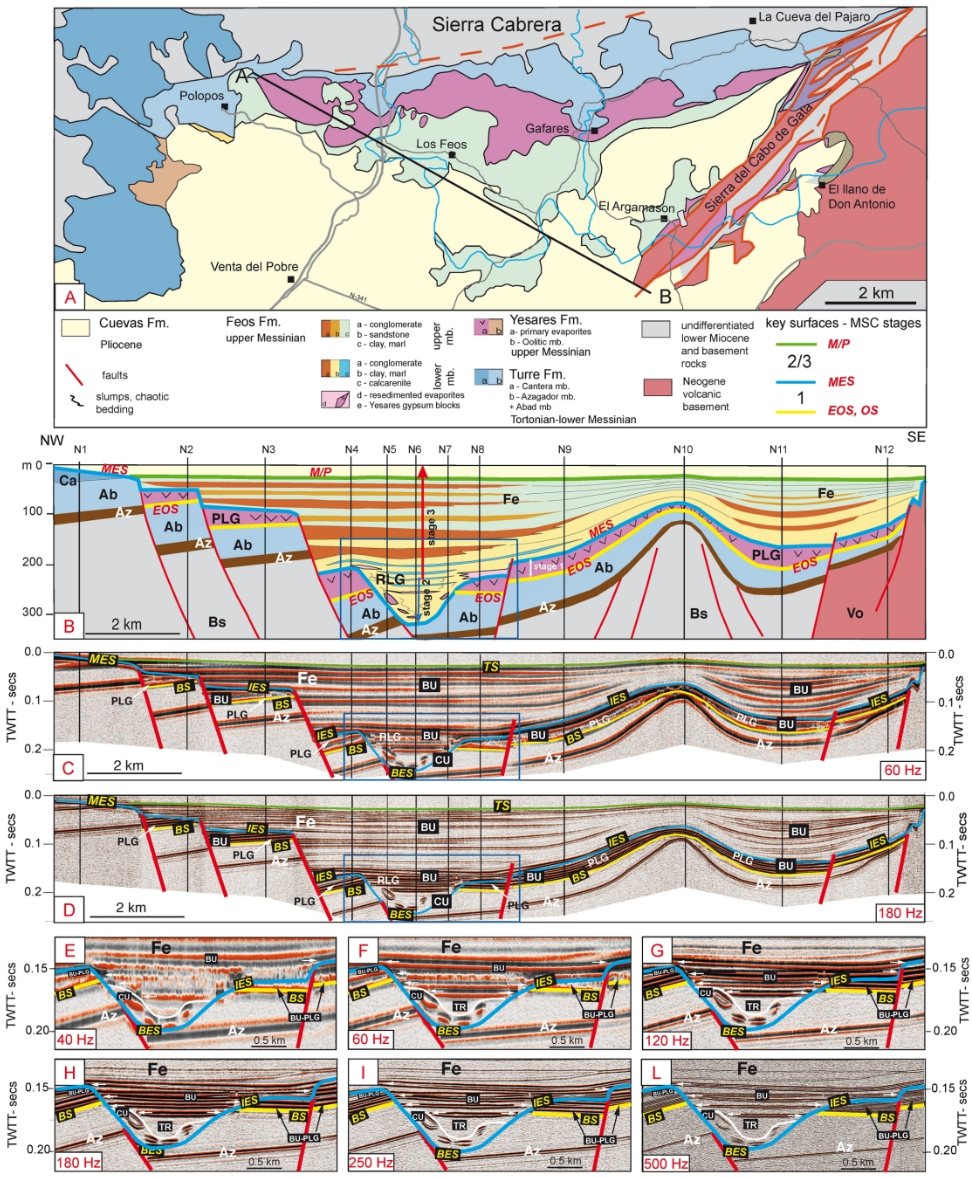

Fig. 10 – Nijar basin synthetic seismic section (see also Fig. 8b); schematic geological map (A) and cross-section in depth domain (B) of the Nijar basin (modified from Omodeo Salé et al., 2012; see location in Fig. 7b) with the location of the hypotethical boreholes used for the reconstruction of synthetic seismic section. C-D) the synthetic seismic section in time domain with different dominant frequency: 60 Hz (C) and 180 Hz (D) resulting in different seismic resolution; black labels show the possible offshore units (white) and surfaces (yellow). Note the complex stratigraphic architecture of the Messinian succession resulting in very close relationships between bedded and chaotic units belonging to the three MSC stages; note in the enlarged area shown at different dominant frequencies (from 40 Hz to 500 Hz) that, without direct observations or borehole data, the BS (placed at the base of in situ PLG deposits) would be cut by an internal erosional surface (IES) passing downslope to the BES; IES and BES would actually represent the downbasin equivalent of the MES, separating MSC stage 1 and 2. At least three BU units can be defined: 1) BU-PLG capped by the MES/IES; 2) BU-RLG within the erosional depression (possibly a canyon or gully head); 3) BU corresponding to stage 3 (=UU, but evaporite-free); at low frequency (40 to 60 Hz) the upper unit shows a seismic facies transparent or with discontinuous reflectors, simulating a chaotic deposit.

199x240mm (300 x 300 DPI)

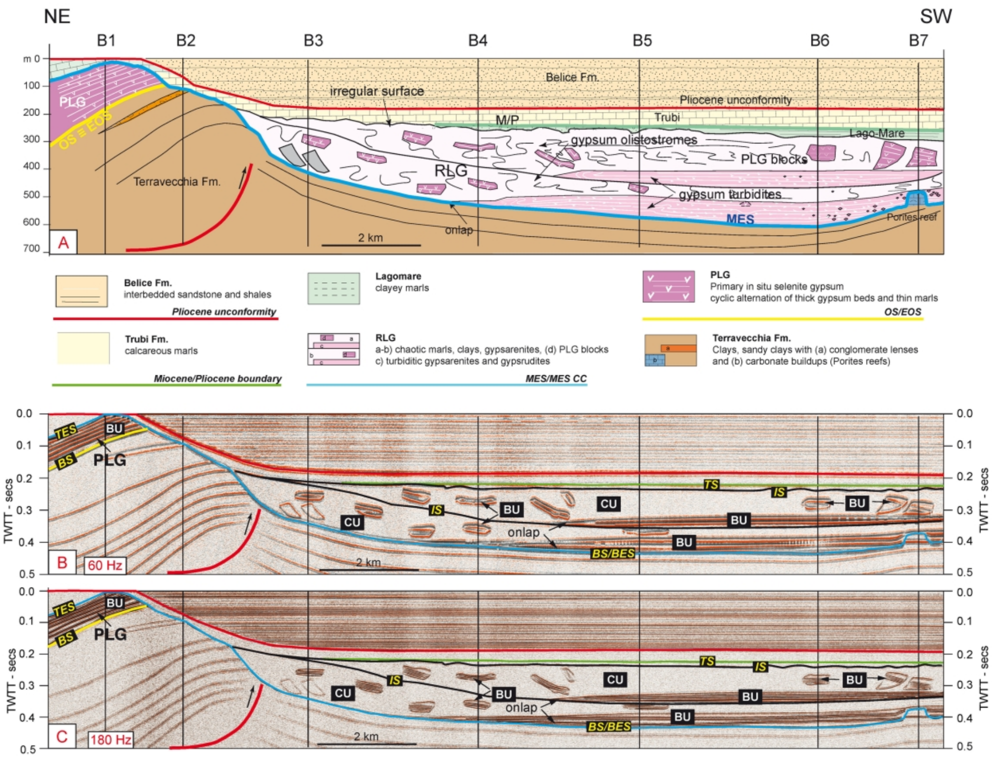

Fig. 11 – Belice synthetic seismic section (see also Fig. 8c); A) cross-section in depth domain of the Belice basin (modified from Roveri et al., 2006; see location in Fig. 4c;); note PLG deposits on top of a thrust-related anticline cut by the MES and resedimented evaporites in the adjoining, deeper sub-basin, forming a complex RLG unit; note also the pre-MSC reef in the deeper basin which underwent strong tectonic subsidence during the Messinian; B–C) the synthetic seismic section in time domain with different dominant frequency: 60 Hz (B) and 180 Hz (C) resulting in different seismic resolution; black labels show the possible offshore units (white) and surfaces (yellow). Note the onlap of BU against the basal surface and an internal surface, the latter marking the top of a chaotic body; BU units in the deeper basin correspond to gypsum turbidites of MSC stage 2; the irregular top of the upper chaotic body could be exchanged for an erosional surface and, due to the very thin Lagomare deposits above it, it could apparently be coincident with the M/P boundary and labeled as TES. Note also the large PLG olistoliths within the chaotic units (compare with photo in Figs 4-5).

215x165mm (300 x 300 DPI)

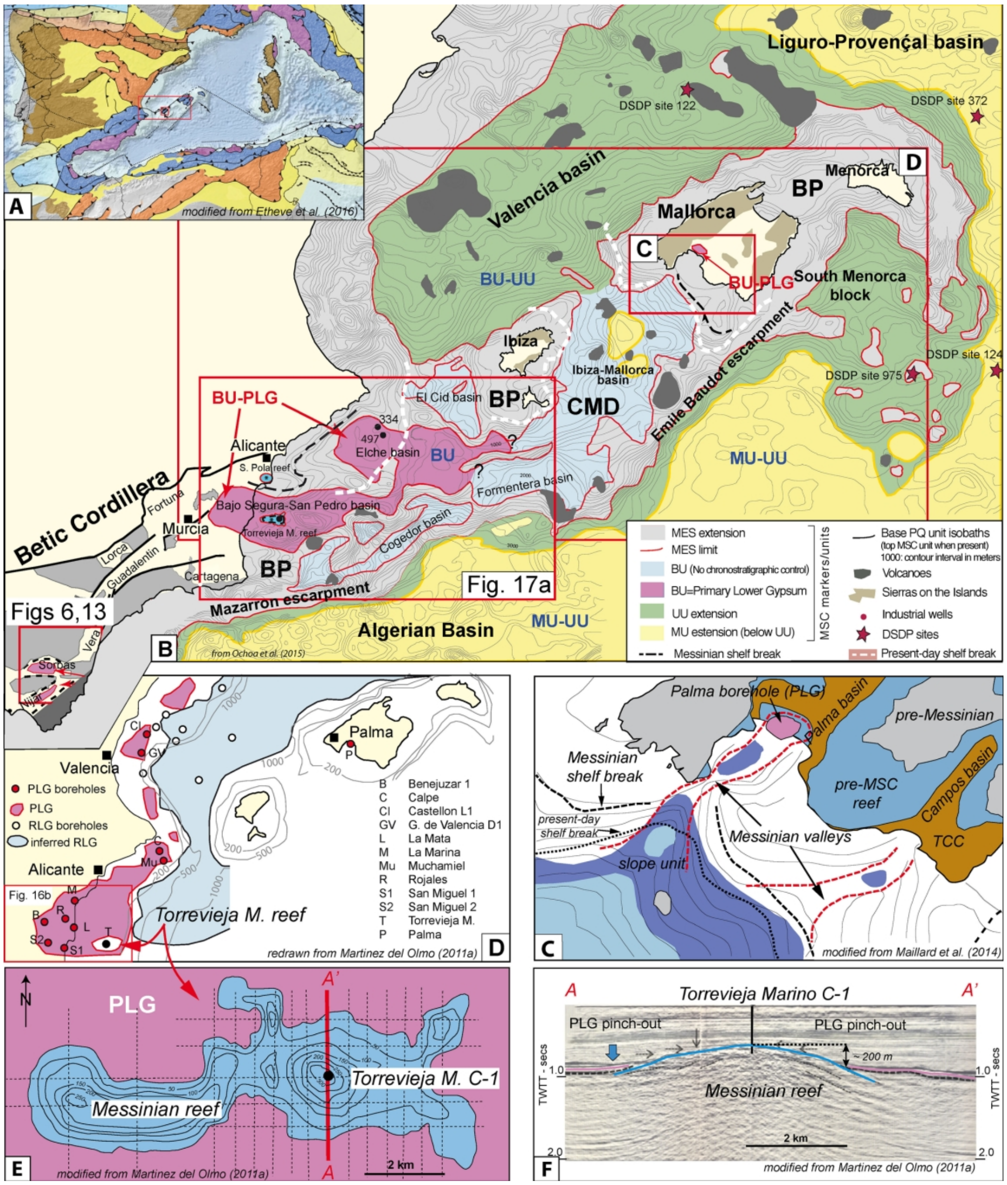

Fig. 12 – Messinian units in the Balearic Promontory area; A) schematic tectonic map of the Western Mediterranean showing the location of the Balearic Promontory; B) present-day distribution of the Messinian units in the Balearic Promontory and adjacent areas (from Ochoa et al., 2015); 334 = Calpe 1 well; 497 = Muchamiel well; MCD = Mallorca Central Depression; BP = Balearic Promontory; CMD = Central Mallorca Depression; PLG = Primary Lower Gypsum unit; note the distribution of inferred PLG deposits in the Elche sub-basin and compare with Fig. 16a; C) location of the PLG evaporites of the Palma sub-basin (from figure 11 of Maillard et al., 2014); the units were deposited in a narrow basin delimited by structural highs and bordered by Messinian reefs; the comparison with B) documents the similarities with the Sorbas Basin in terms of size and overall stratigraphic architecture; D) the distribution of PLG evaporites in the Balearic Promontory and Valencia Basin according to Martinez Del Olmo (2011); E) the Torrevieja Marino Messinian reef (see location in D); contour lines refer to the elevation of reef deposits above the highest onlap of PLG evaporites; seismic lines across the reef (F) show the 360° onlap of PLG evaporites against the reef front; difference in elevation between the reef top and the gypsum suggest an original paleodepth of around 200 m.

180x212mm (300 x 300 DPI)

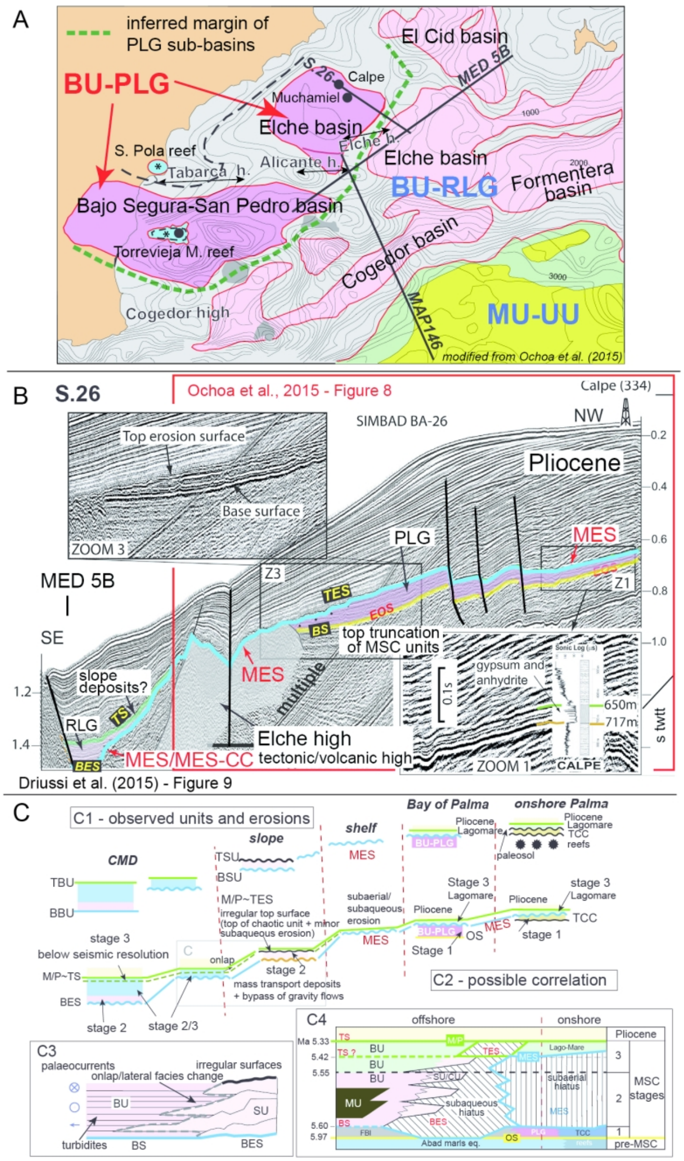

Fig. 13 – A - close-up of the map of Ochoa et al. (2015) shown in Fig. 12B modified in the Elche sub-basin area, based on our interpretation of the seismic profile SIMBAD 26 (S.26); the trace of this seismic profile is taken from Driussi et al., 2015. This sub-basin is subdivided by a NE-SW oriented structural high (the Elche high) in two sectors with the PLG evaporites to the NW and a MSC unit floored by the MES to the SE (possibly corresponding to MSC stage 2 RLG unit and overlying stage 3 deposits); the green dotted line represents the inferred PLG southern basin margin, while the black dotted line interpreted by Ochoa et al. (2015) as the Messinian shelf break represents its northern margin; B – interpretation of the SIMBAD 26 seismic profile shown in Driussi et al. (2015); note the Messinian unit in the southeastward end of the profile; the PLG unit (in violet) shows a lower concordant base; it is cut on top by the Messinian erosional surface (MES) and occurring upslope of the area deformed and eroded possibly corresponding to the Elche structural/volcanic high; beyond this structure, the Messinian unit (in cyan) shows a basal unconformity (MES or MES-CC) and onlap terminations against the eroded area; note the rapid thinning of layered deposits and the probable transition to slope deposits. The two Messinian units were likely deposited in different times in areas separated by a structural/volcanic feature pre-existing and/or uplifted during and

still active after the MSC; C - Schematic stratigraphic relationships between the MSC units recognized in the Balearic Promontory (modified from Maillard et al., 2014). C1 – observed units and surfaces; C2-C4 - new interpretation model with the MES developing on top of the BU-PLG unit and passing downslope to the BES at the base of the Slope and BU units; C3 – detail of the possible facies relationships between the stratified deposits of the BU (likely turbiditic) and the chaotic deposits of the Slope Unit; note that the overall onlap of the BU deposits on the Slope unit is not necessarily related to a different age of the two units and that the top of the latter is an irregular surface, which does not necessarily correspond to a subaerial unconformity. CMD = Central Mallorca Depression.

175x208mm (300 x 300 DPI)

The synthetic seismic expression of Messinian salinity crisis onshore records: implications for shallow- to deep-water correlation

Roveri M[a,*], Gennari R.[a], Ligi M.[b], Lugli S.[c], Manzi V.[a], Reghizzi, M.[a]

Supporting Information

1. Data and methods

1.1 Seismic modelling

In order to assess complexity and possible pitfalls in interpretation of seismic reflection sections crossing evaporitic basins, three locations have been selected for seismic forward modelling. The selected geological sections (Sorbas, Nijar and Belice; Fig. 8 a,b,c of the main text, respectively) include alternation of high and low velocity layers (marls, evaporites and shales, limestones, sandstones and conglomerates), erosional surfaces, steeply dipping prograding features, faulted blocks, synclines and anticlines. For the different lithologies we have used average density and P-wave velocity values from the literature (values adopted reported in Table 2 of the main text). The selected surfaces are stratigraphic surfaces derived from measured sections in the area, field observations and data from the literature. A number of forward modelling methods are available, and the choice of method generally depends on a trade-off between the accuracy necessary and the desired computing time. There are two classes of seismic modeling: ray tracing and wave equation methods. Implementation of both classes exists for one, two, and three dimensions; shot gathers; common midpoint (CMP) gathers; and stacked data simulation. Ray methods usually give very accurate traveltimes and accurate amplitudes for geometric arrivals if the model is sufficiently smooth (Hubral, 1977). These methods are efficient, and computing time is low to moderate. Diffractions and multiple reflections are not modelled. Wave equation methods solve the propagation problem over the entire model, rather than performing local solutions as in ray methods (Hilterman, 1970; Kelley et al., 1976).

We simulated stacked seismic sections adopting the image rays approximation (Fagin, 1991), that uses zero-offset traveltime modelling based on normal incidence ray tracing. It is a very useful and trivially simple tool for understanding reflectors complexity in field data (Yilmaz, 2001). Ray theory uses the fact that energy in the form of seismic rays travels along minimum time paths in the model. As in optics, rays bend when velocities change, obeying Snell's law, and are partially reflected when velocity or density discontinuities are encountered. Traveltimes of reflected arrivals correspond to the times of the minimum time paths, while amplitudes are a combination of geometric spreading and reflection coefficients. The reflection coefficient, based on the Zoeppritz equations for elastic media, depends on the velocities and densities on both sides of the interface. The normal-incidence reflection coefficient can be expressed as (Dobrin, 1952):

$$R_i = \frac{(\rho_{i+1} v_{i+1} - \rho_i v_i)}{(\rho_{i+1} v_{i+1} + \rho_i v_i)} \qquad (1)$$

where: ρ = rock density; *υ* = seismic velocity; with *i* and *i+1* representing parameters above and below the i-th interface, respectively.

Once a geological model has been built including depth smooth horizons, P-wave velocities and densities, a synthetic seismogram can be constructed to identify seismic reflections. The steps necessary to create a synthetic seismogram are (Coffen, 1978): *1)* calculate vertical reflection times using normal incidence ray tracing; *2)* calculate reflection coefficients R_o using eq. 1 for each horizon; *3)* combine the last two items to create a reflection coefficient time series $R_0(t)$; *4)* convolve the reflection coefficient series with a source wavelet *w(t)*. The source signal we used is a 3 parameters Gabor wavelet defined as:

$$w(t) = \Re e\left\{ A \exp\left[-\left(\frac{2\pi f_M t}{\gamma} \right)^2 \right] \exp(2\pi i f_M t + \varphi) \right\} \qquad \forall t \in \left[-\frac{T}{2}, \frac{T}{2} \right] \qquad (2)$$

where: *A* is a constant and $i^2=-1$; f_M is the dominant frequency of the signal; φ is the initial phase; γ is a parameter that determines the complexity of the waveform and T is the length of the wavelet. We adopted a zero phase wavelet ($\varphi = 0$) and $\gamma = 3$ that simulates a zero-phase Richer wavelet. Several dominant frequencies (f_M = 40, 60, 120, 180, 250 and 500 Hz) have been used for testing vertical resolution. Finally, we added 5% white noise *n(t)* to the computed seismic traces to simulate uncoherent noise during real data acquisition. Thus, the final simulated seismic trace can be summarized by the convolutional model:

$$T(t) = R_0(t) * w(t) + n(t) \qquad (3).$$

Synthetic traces with constant spacing are collected into a true zero-offset section. Finally, the zero-offset section is time migrated in order to locate correctly reflections at depth. Several synthetic sections with different CDPs' spacing (3.125, 6.25, 12.5 and 25 m) have been created in order to test horizontal resolution with common seismic reflection acquisition geometries. Seismic data were stored on disk in SEG-Y format with a sampling rate of 0.25 ms and a record length of 1s. Post-stack time migration was carried out using an industrial package (Disco/Focus) by Paradigm Geophysical and was achieved by a finite difference approximation to the wave equation (Claerbout and Doherty, 1972), using a velocity model obtained from velocities determining reflection coefficients. A variable colour density display has been created by assigning different densities of shading to different amplitude values (positive, black; negative, red). Higher amplitudes are shaded darker, while lower amplitudes are less dark.

1.2 Sr isotopes

The gypsum samples collected in the Sorbas-Vera basin and in the Bajo Segura basin (Fig. S1) were processed for Sr isotope analysis at the Isotope Geochemistry Laboratory at the Department of Chemical and Geological Sciences of the University of Modena and Reggio Emilia. Small portions of different crystals were isolated and splitted along the major cleavage planes. The fresh surfaces exposed were washed with abundant MilliQ water. Then, 10 mg of gypsum powder were obtained from each sample using a 0.5 mm steel bit handheld driller, taking care to abrade only limited and transparent portions of the crystals in order to avoid the presence of detrital inclusion in the final target material. Samples were leached using 1M ammonium acetate to remove exchangeable Sr and then washed and centrifuged with MilliQ water. After drying, samples were completely dissolved with 3N HNO_3. The solutions were loaded into 300 μL columns containing Eichrom Sr-SPEC resin SR-B50-A (100-150 μm) to remove matrix and isolate Sr from interfering elements Ca, Rb, REE, following the procedure reported in Palmiotto et al. (2013). Final solutions were adjusted to a concentration of 4% w/w HNO_3 and analyzed within a few days. Strontium isotope ratios were obtained using a high resolution multi collector inductively coupled plasma mass spectrometer (HR-MC-ICPMS *Thermo Scientific™ Neptune*), housed at CIGS (Centro Interdipartimentale Grandi Strumenti, University of Modena and Reggio Emilia). Sample solutions were introduced into the Neptune using a PFA 100 μL/min nebulizer and a quartz cyclonic + Scott type spray chamber. The sensitivity for 250 ppb Sr was >8 V on the ^{88}Sr peak and the blank level (4% w/w HNO_3) was < 0.007 V. The strontium isotope standard NIST SRM 987, with a generally accepted $^{87}Sr/^{86}Sr$ of 0.710260 ± 0.000020 (Ehrlich et al., 2001) has been used as an external standard (the uncertainty is expressed as twice the standard deviation, 2 S.D.). Samples, standards and blank solutions were analyzed using the same instrument configuration, bracketing sequence and mathematical/statistical corrections described in Reghizzi et al. (2017). The obtained values (Fig. S1) were normalized to the NIST SRM 987 value of 0.710248 used by McArthur et al. (1994, 2001) as reference standard for the reconstruction of the global ocean Sr curve. Repeated measurements of the NIST SRM 987 yielded a mean value of 0.710271 ± 0.000021 (2 S.D., n = 28). The internal precision on individual standard analyses varied between 0.000006 and 0.000009 (twice the standard error – 2 S.E.). For all the samples analyzed the instrument gave an average internal uncertainty value of 0.000008 (2 S.E.), with a minimum value of 0.000007 and a maximum of 0.000010.

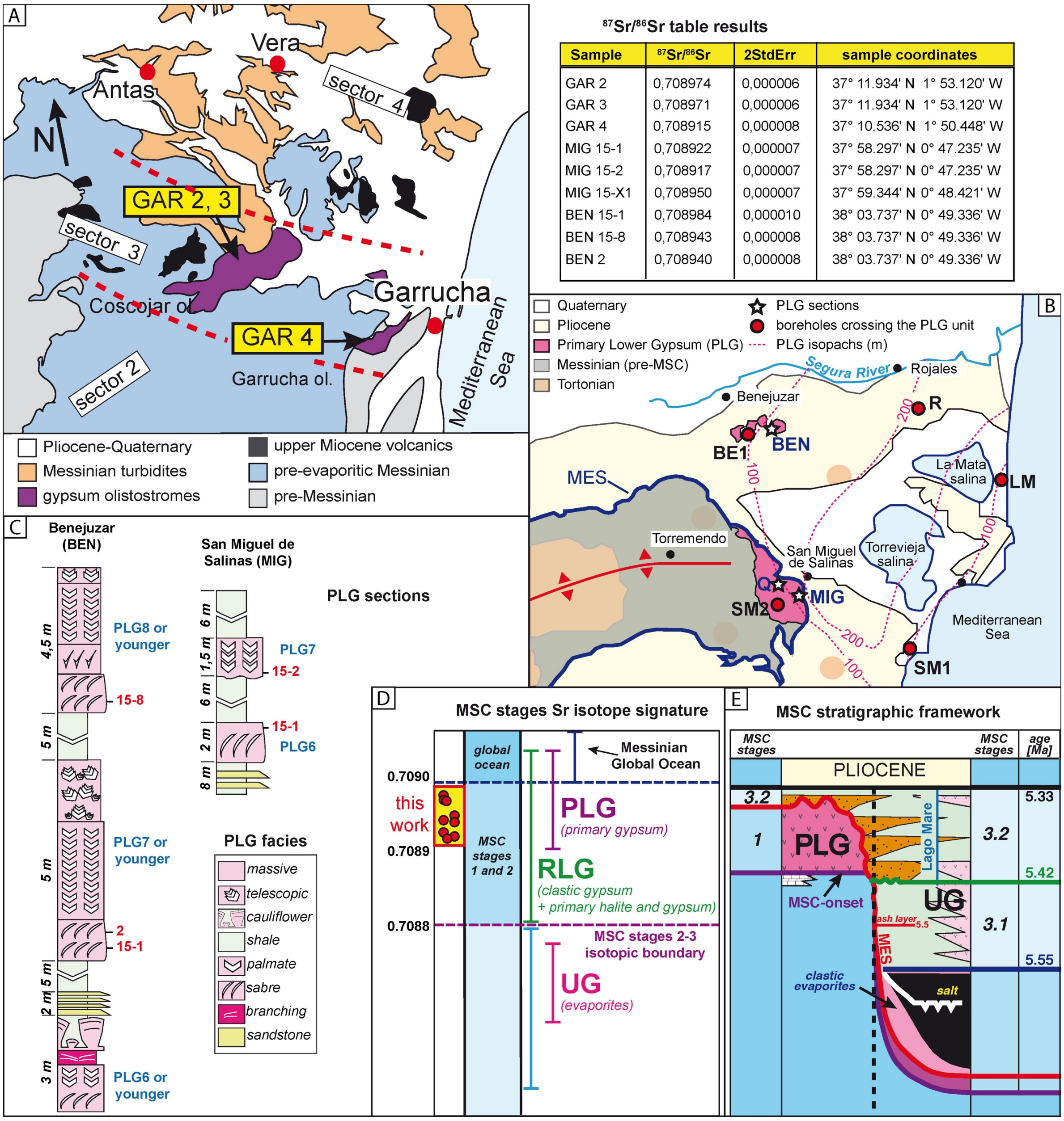

$^{87}Sr/^{86}Sr$ table results

Sample	$^{87}Sr/^{86}Sr$	2StdErr	sample coordinates
GAR 2	0,708974	0,000006	37° 11.934' N 1° 53.120' W
GAR 3	0,708971	0,000006	37° 11.934' N 1° 53.120' W
GAR 4	0,708915	0,000008	37° 10.536' N 1° 50.448' W
MIG 15-1	0,708922	0,000007	37° 58.297' N 0° 47.235' W
MIG 15-2	0,708917	0,000007	37° 58.297' N 0° 47.235' W
MIG 15-X1	0,708950	0,000007	37° 59.344' N 0° 48.421' W
BEN 15-1	0,708984	0,000010	38° 03.737' N 0° 49.336' W
BEN 15-8	0,708943	0,000008	38° 03.737' N 0° 49.336' W
BEN 2	0,708940	0,000008	38° 03.737' N 0° 49.336' W

Fig. S1 – Table with the 87Sr/86Sr values obtained from selenite gypsum samples analysed in this work: all the values fall in the range of the first stage of the salinity crisis. (A) simplified geological map of the Garrucha-Coscojar area of the Sorbas-Vera basin (see Fig. 7b of the main text) with the location of the samples; (B) simplified geological map of the Bajo Segura basin with the location of the main outcrop sections and boreholes crossing the PLG deposits; (C) Sedimentary logs of the Benejuzar and San Miguel de Salinas sections showing the location of samples for Sr isotope analysis; (D) Strontium isotope values framed in the Messinian Sr isotope stratigraphy; (E) stratigraphic framework of the MSC (modified from Manzi et al., 2013 and Roveri et al., 2014a)

References

CLAERBOUT, J.F. & DOHERTY, S.M. (1972) Downward continuation of moveout-corrected seismograms. *Geophysics*, 37, 741–768.

COFFEEN, J.A. (1978) *Seismic Exploration Fundamentals: Seismic Techniques for Finding Oil*. Pennwell Corporate, Tulsa, Oklahoma, pp. 360.

DOBRIN, M.B. (1952) *Introduction to Geophysical Prospecting*. McGraw-Hill, New York-London, pp. 435.

EHRLICH, S., GAVRIELI, I., DOR, L. & HALICZ, L. (2001). Direct high-precision measurements of the $^{87}Sr/^{86}Sr$ isotope ratio in natural water, carbonates and related materials by multiple collector inductively coupled plasma mass spectrometry (MC-ICP-MS). *Journal of Analytical Atomic Spectrometry*, 16, 1389-1392.

FAGIN, S.W. (1991) *Seismic Modeling of Geologic Structures: Applications to Exploration Problems*. Society of Exploration Geophysicists, Tulsa, Oklahoma. Geophysical Development Series 2.

HILTERMAN, F.J. (1970) Three-dimensional seismic modelling. *Geophysics*, 35, 1020–1037.

HUBRAL, P. (1977) Migration: Some ray theoretical aspects. *Geophysical Prospecting*, 25, 739–745.

KELLEY, K.R., WARD, R.W., TREITEL, S. & ALFORD, R.M. (1976) Synthetic seismograms – a finite difference approach. *Geophysics,* 41, 2–27.

MAILLARD, A., DRIUSSI, O., LOFI, J., BRIAIS, A., CHANIER, F., HÜBSCHER, C. & GAULLIER, V. (2014) Record of the Messinian Salinity Crisis in the SW Mallorca area (Balearic Promontory, Spain). *Marine Geology*, 357, 304–320.

MCARTHUR, J. M., HOWARTH, R. J. & BAILEY, T. R. (2001). Strontium isotope stratigraphy: LOWESS version 3: best fit to the marine Sr-isotope curve for 0-509 Ma and accompanying look-up table for deriving numerical age. *The Journal of Geology*, 109, 155-170.

MCARTHUR, J.M. (1994). Recent trends in strontium isotope stratigraphy, Terra Nova, 6, 331 – 358.

PALMIOTTO, C., CORDA, L., LIGI, M., CIPRIANI, A., DICK, H.J.B., DOUVILLE, E., GASPERINI, L., MONTAGNA, P., THIL, F., BORSETTI, A.M., BALESTRA, B. & BONATTI, E. (2013). Nonvolcanic tectonic islands in ancient and modern oceans. *Geochemistry, Geophysics, Geosystems*, 14(10):4698–4717.

REGHIZZI, M., GENNARI, R., DOUVILLE, E., LUGLI, S., MANZI, V., MONTAGNA, P, ROVERI, M., SIERRO, F. J. & TAVIANI, M. (2017). Isotope stratigraphy ($^{87}Sr/^{86}Sr$, $\delta^{18}O$, $\delta^{13}C$) of the Sorbas basin (Betic Cordillera, Spain): paleoceanographic evolution across the onset of the Messinian salinity crisis. *Palaeogeography, Palaeoclimatology, Palaeoecology*, 469, 60-73.

STEIN, M., STARINSKY, A., KATZ, A., GOLDSTEIN, S. L., MACHULUS, M. & SCHRAMM, A. (1997) Strontium isotopic, chemical and sedimentological evidence for the evolution of Lake Lisan and the Dead Sea. *Geochimica et Coscmochimica Acta*, 61, 3975-3992.

YILMAZ, Ö. (2001) *Seismic Data Analysis: Processing, Inversion, and Interpretation of Seismic Data*. Society of Exploration Geophysicists, Tulsa, Oklahoma. Geophysical Development Series 10.